Cell Stem Cell

Article

Rapid generation of functional vascular organoids via simultaneous transcription factor activation of endothelial and mural lineages

Graphical abstract

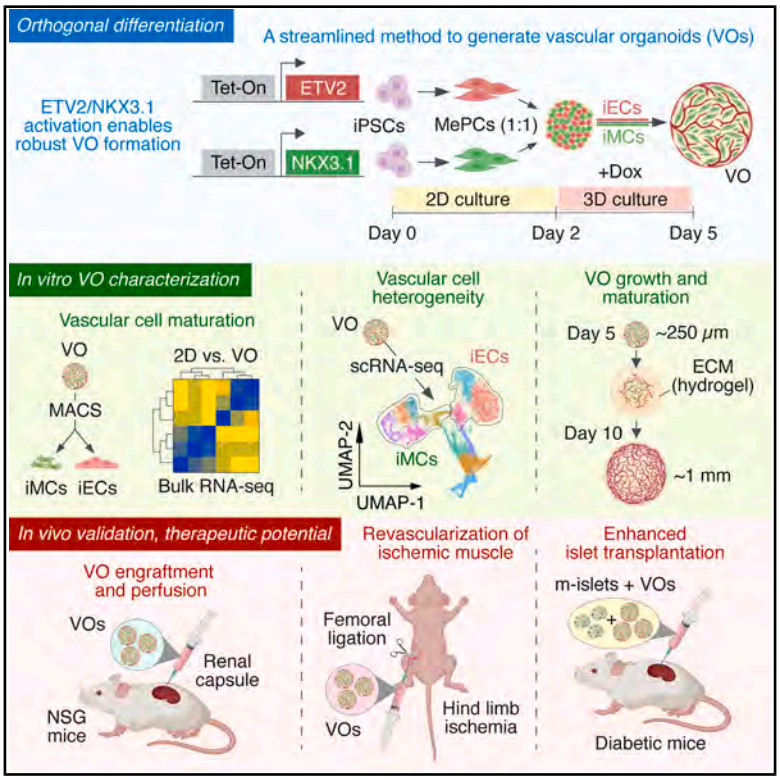

Highlights

- Rapid generation of vascular organoids from iPSCs via orthogonal TF activation
- Simultaneous iEC and iMC differentiation drives mature, functional vessel formation
- TF activation timing modulates vascular cell identity and heterogeneity
- Vascular organoids engraft and revascularize ischemic and transplant models

Authors

Liyan Gong (公丽岩), Yadong Zhang, Yonglin Zhu (朱咏林), ..., Kaifu Chen, Kai Wang (王凯), Juan M. Melero-Martin

Correspondence

kai.wang88@pku.edu.cn (K.W.), juan.meleromartin@childrens.harvard.edu (J.M.M.-M.)

In brief

Melero-Martin and colleagues developed a rapid method to generate vascular organoids from human iPSCs by orthogonally activating the transcription factors ETV2 and NKX3.1. This strategy enabled controlled co-differentiation of vascular cells and supported *in vivo* engraftment, offering a versatile platform for vascular biology, tissue engineering, and regenerative medicine.

Gong et al., 2025, Cell Stem Cell *32*, 1–18
August 7, 2025
https://doi.org/10.1016/j.stem.2025.05.014

CellPress

Cell Stem Cell

CellPress

Article

Rapid generation of functional vascular organoids via simultaneous transcription factor activation of endothelial and mural lineages

Liyan Gong (公丽岩),[1,2] Yadong Zhang,[3,4] Yonglin Zhu (朱咏林),[1,2] Umji Lee,[1,2] Allen Chilun Luo,[1] Xiang Li (李想),[1,2] Xi Wang (王茜),[5] Danyang Chen (陈丹阳),[3] William T. Pu,[3,7] Ruei-Zeng Lin,[1,2] Minglin Ma,[5] Miao Cui,[3] Kaifu Chen,[3,4] Kai Wang (王凯),[1,2,6,*] and Juan M. Melero-Martin[1,2,7,8,*]

[1]Department of Cardiac Surgery, Boston Children's Hospital, Boston, MA 02115, USA
[2]Department of Surgery, Harvard Medical School, Boston, MA 02115, USA
[3]Department of Cardiology, Boston Children's Hospital, Boston, MA 02115, USA
[4]Department of Pediatrics, Harvard Medical School, Boston, MA 02115, USA
[5]Department of Biological and Environmental Engineering, Cornell University, Ithaca, NY 14853, USA
[6]Department of Physiology and Pathophysiology, School of Basic Medical Sciences, State Key Laboratory of Vascular Homeostasis and Remodeling, Beijing Advanced Center of Cellular Homeostasis and Aging-Related Diseases, Peking University, Beijing 100191, China
[7]Harvard Stem Cell Institute, Cambridge, MA 02138, USA
[8]Lead contact
*Correspondence: kai.wang88@pku.edu.cn (K.W.), juan.meleromartin@childrens.harvard.edu (J.M.M.-M.)
https://doi.org/10.1016/j.stem.2025.05.014

SUMMARY

Vascular organoids (VOs) are valuable tools for studying vascular development, disease, and regenerative medicine. However, controlling endothelial and mural compartments independently remains challenging. Here, we present a streamlined method to generate VOs from induced pluripotent stem cells (iPSCs) via orthogonal activation of the transcription factors (TFs) ETV2 and NKX3.1 using Dox-inducible or modRNA systems. This approach enables efficient co-differentiation of endothelial cells (iECs) and mural cells (iMCs), producing functional 3D VOs in 5 days without ECM embedding. VOs matured further upon ECM exposure, forming larger, structured vessels. Single-cell RNA sequencing revealed vascular heterogeneity, and temporal regulation of TF expression allowed modulation of arterial and angiogenic iEC phenotypes. *In vivo*, VOs engrafted into immunodeficient mice, formed perfused vasculature, and promoted revascularization in models of hind limb ischemia and pancreatic islet transplantation. These findings establish a rapid and versatile VO platform with broad potential for vascular modeling, disease studies, and regenerative cell therapy.

INTRODUCTION

Blood vessels are essential to nearly all tissues, delivering nutrients and oxygen, regulating hemostasis, and modulating inflammation.[1] During development, vasculature shapes organ formation[2–4] and supports postnatal tissue growth and repair.[5,6] Vascular niches also maintain stem cell populations.[7–9] Recreating functional vascular networks is therefore foundational to both basic and translational vascular biology.[10,11]

Functional blood vessels require two key cell types: endothelial cells (ECs) and perivascular mural cells (MCs).[12,13] Identifying reliable sources of these cells has been central to vascular engineering.[14] Initial approaches relied on isolating primary cells from vessels, which has limited applicability. Alternatives such as endothelial colony-forming cells (ECFCs) and mesenchymal stem cells (MSCs) offer access to EC and MC progenitors,[15–19] but their scarcity and reduced function in disease limit clinical utility in autologous settings.[14,15,20] Induced pluripotent stem cells (iPSCs) have transformed the field, providing scalable, autologous sources of vascular cells.[21,22] Protocols to derive iECs and iMCs continue to improve,[23–25] expanding therapeutic possibilities.

A major challenge, however, is the immaturity of iPSC-derived cells, which limits *in vivo* engraftment and functionality.[26,27] Although multiple protocols have been developed to differentiate ECs and MCs independently[28–32]—using either chemically defined factors[28,29] or transcription factors (TFs)[30,31,33,34]—the development of these two lineages *in vivo* is tightly coordinated. Vascular maturation depends on EC-MC interactions through signaling pathways such as PDGFB, Notch, and TGF-β.[1,12,35] Co-differentiation of ECs and MCs remains difficult because of their distinct and often incompatible culture requirements.

Embryoid body (EB) models have long been used to induce spontaneous vascular differentiation,[36] but they offer limited

Please cite this article in press as: Gong et al., Rapid generation of functional vascular organoids via simultaneous transcription factor activation of endothelial and mural lineages, Cell Stem Cell (2025), https://doi.org/10.1016/j.stem.2025.05.014

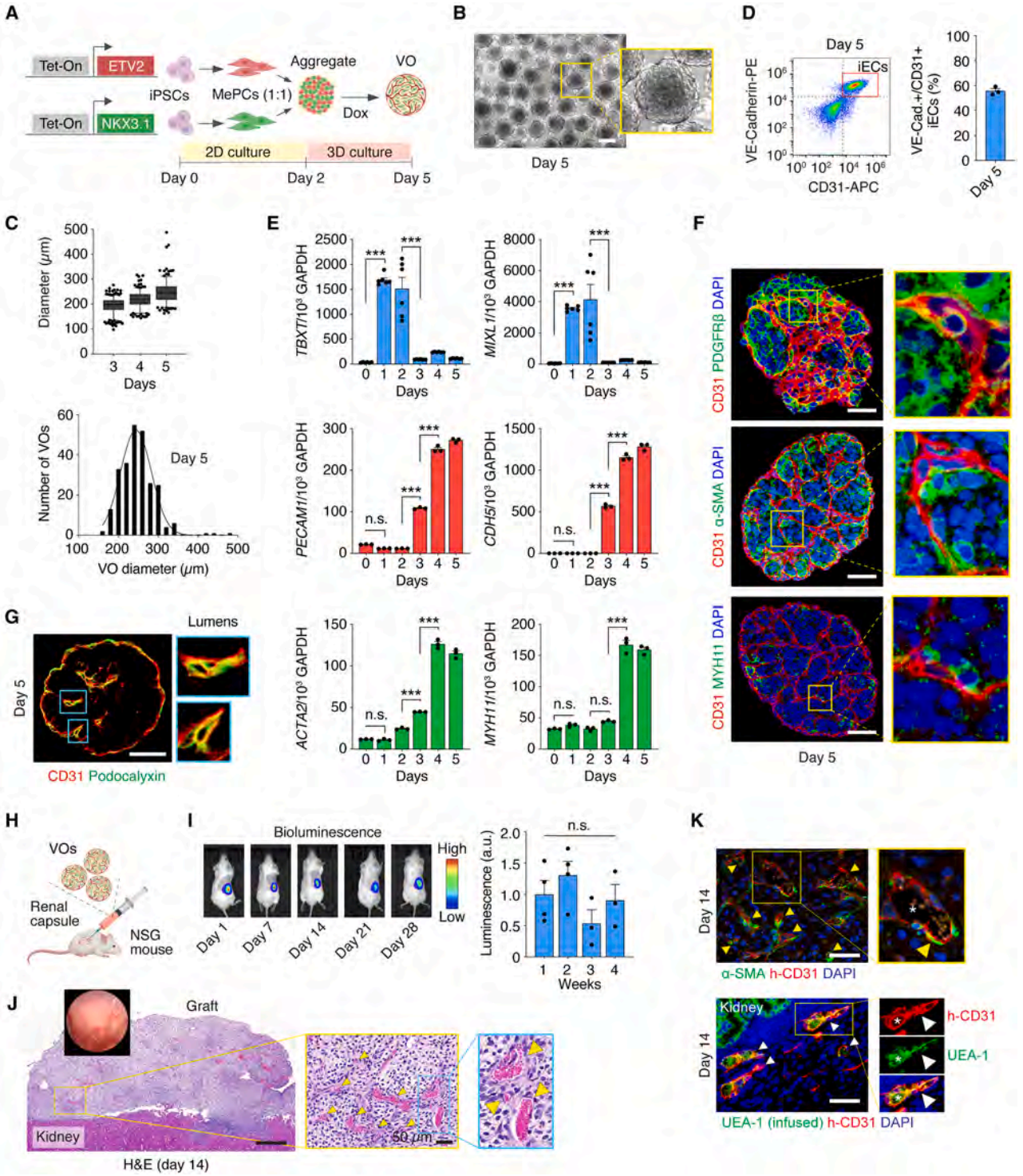

Figure 1. Generation and *in vivo* engraftment of vascular organoids via ETV2 and NKX3.1 activation

(A) Schematic of the two-step protocol for generating vascular organoids (VOs) from iPSCs. Stage 1: differentiation of iPSCs into MePCs in 2D. Stage 2: 3D aggregation of MePCs and Dox induction of ETV2 and NKX3.1 leading to VO generation.

(B) Bright-field image of VOs at day 5.

(C) VO diameter over days 3–5 (top) and size distribution at day 5 (bottom). Data shown as box-and-whisker plot, where whiskers represent the 5th–95th percentile range, and dots correspond to VOs with sizes outside this range ($n > 200$).

(D) Flow cytometry of VE-Cadherin and CD31 at day 5 (left) with quantification of $CD31^+/VE\text{-}Cadherin^+$ iECs (right) ($n = 3$).

(legend continued on next page)

Please cite this article in press as: Gong et al., Rapid generation of functional vascular organoids via simultaneous transcription factor activation of endothelial and mural lineages, Cell Stem Cell (2025), https://doi.org/10.1016/j.stem.2025.05.014

control over cellular composition. Recent strategies have introduced vascular organoids (VOs) for disease modeling.[37–39] However, these VOs still rely on the spontaneous emergence of MCs, limiting control over their cellular composition, and are not optimized for therapeutic use—often requiring extracellular matrix components such as Matrigel, prolonged culture periods (~3 weeks), and lacking scalability.

Here, we present a method to generate VOs from human iPSCs through orthogonal activation of the vascular fate-determining TFs ETV2 and NKX3.1, enabling independent and synchronous differentiation of iECs and iMCs. This approach produces large numbers of uniform VOs in just 5 days, featuring robust vascular development, including lumenized vessels with apical-basal polarity and diverse, mature vascular cell populations. When transplanted *in vivo*, these VOs formed perfused human vasculature and improved tissue perfusion in models of hindlimb ischemia. This method provides a versatile platform for studying vascular assembly and holds translational potential in regenerative medicine.

RESULTS

Generation of VOs through orthogonal activation of TFs

We previously developed 2D protocols to generate iECs and iMCs from iPSCs via transient activation of the vascular TFs ETV2 and NKX3.1, respectively.[30,31,40] Building on this, we investigated whether iPSCs could be co-differentiated into both lineages in a 3D configuration to form VOs (Figure 1A). We used engineered human dox-ETV2-iPSC and dox-NKX3.1-iPSC lines, which were first differentiated into mesoderm progenitor cells (MePCs) over 2 days using GSK-3β inhibition. These MePCs were combined at a 1:1 ratio, aggregated in non-adherent plates on an orbital shaker, and exposed to doxycycline (Dox) for 3 days (Figure 1A). This approach generated thousands of uniformly sized VOs in just 5 days, each with an average diameter of ~250 μm (Figures 1B and 1C).

The dual TF strategy enabled concurrent differentiation of iPSCs into iECs and iMCs. After 3 days of Dox exposure, ~50% of cells were VE-Cadherin$^+$/CD31$^+$ iECs (Figure 1D). Immunofluorescence confirmed robust induction of ETV2 and NKX3.1 during differentiation (Figure S1), while mesodermal markers TBXT and MIXL1 declined following Dox treatment (Figures 1E and S1). By day 5, VOs contained iECs expressing *CDH5* and *PECAM1* (Figure 1E) organized into CD31$^+$ vascular networks (Figure 1F), and iMCs expressing *ACTA2* and *MYH11* (Figure 1E). Spatially, CD31$^-$/PDGFRβ$^+$ iMCs were interstitially distributed, with some α-SMA$^+$/MYH11$^+$ cells adjacent to endothelial-lined structures (Figure 1F). These CD31$^+$ cords displayed early lumen formation, not yet open or perfused, but structurally consistent with nascent vessels. iECs showed correct apical-basal polarity, with podocalyxin marking the luminal surface (Figure 1G).

Next, we assessed the capacity of the VOs to become perfused *in vivo*. To this end, we employed a renal capsule implantation model in immunodeficient NSG mice, implanting 1,000 VOs per mouse (Figure 1H). Engraftment of the VOs was monitored using a luciferase reporter expressed in the endothelial compartment. Bioluminescent imaging confirmed that VOs successfully engrafted for several weeks, remained localized at the transplantation site, and maintained iEC presence without notable loss (Figure 1I). By day 14, analysis of explanted tissue revealed formation of highly vascularized grafts. Histology showed extensive networks of perfused vessels (Figure 1J), predominantly lined by human iECs, as indicated by human-specific CD31 expression (Figures 1K and S1), and containing mouse erythrocytes—evidence of anastomosis with the host vasculature. Human vessels were surrounded by α-SMA$^+$ iMCs, consistent with vessel maturation. Perfusion was confirmed by tail vein infusion of UEA-1, a lectin that selectively binds human ECs, detected within vessel lumens at the time of infusion (Figure 1K).

Taken together, this dual TF-driven VO methodology not only facilitated the orthogonal differentiation of iECs and iMCs but also promoted their interaction, resulting in the formation of a spatially organized vascular network that demonstrated the capacity to become perfused upon *in vivo* implantation.

VO differentiation facilitates vascular cell maturation

To assess gene expression, VOs were dissociated into single cells and sorted by CD31 expression: CD31$^+$ cells were designated VO-iECs, and CD31$^-$ cells as VO-iMCs. These were compared with 2D-iECs and 2D-iMCs generated via monolayer protocols as non-co-cultured controls (Figure 2A).

Bulk RNA-seq analysis revealed thousands of differentially expressed genes (DEGs; $\log_2$ fold change > 2; $p < 10^{-2}$) between VO-derived and 2D vascular cells (Figure 2A). Hierarchical clustering and principal-component analysis (PCA) showed that VO-iECs clustered closer to 2D-iECs than to any iMC group (Figure 2B). In contrast, VO-iMCs displayed greater transcriptional divergence from 2D-iMCs, suggesting that co-differentiation in 3D exerts a stronger influence on MC identity. This divergence may reflect sustained proximity to iECs during differentiation, as endothelial interactions are known to promote MC heterogeneity and maturation.[31]

(E) qPCR analysis of mesoderm (*TBXT* and *MIXL1*), endothelial (*PECAM1* and *CDH5*), and mural markers (*ACTA2* and *MYH11*) during differentiation (n = 3–6; ***$p < 0.001$).
(F) Immunofluorescence of VOs at day 5 showing endothelial (CD31$^+$, red), mural (PDGFRβ$^+$, green), and smooth muscle (α-SMA$^+$, green; MYH11$^+$, green) cells.
(G) Early-stage lumen formation in CD31$^+$ vascular structures, indicated by apical podocalyxin (green) localization on the luminal surface of iEC-lined cords. These vessels exhibit proper polarity but remain non-perfused at this stage.
(H–K) *In vivo* engraftment of VOs containing a luciferase reporter in the iEC compartment. (H) Schematic of the renal capsule transplantation model in NSG mice. (I) Bioluminescence imaging of transplanted VOs at weekly intervals (left) with quantification of signal intensity (right) (n = 3–4). (J) H&E staining on day 14 showing a representative VO graft and the presence of numerous perfused microvessels (yellow arrowheads). (K) Immunofluorescence of human CD31$^+$ vessels and α-SMA$^+$ perivascular cells in the graft (yellow arrowheads), with perfused vessels confirmed by colocalization of perfused UEA-1 and h-CD31 staining (white arrowheads).
All data are mean ± SEM. (D, E, and I). n are biological replicates (D, E, and I) and individual VOs (C). Statistics are one-way ANOVA with Bonferroni's post-test analysis (E and I). Scale bars: 50 μm (F, G, K, and J right), 200 μm (B), and 400 μm (J left). (A) and (H) were partially created with BioRender.com.
See also Figure S1.

Please cite this article in press as: Gong et al., Rapid generation of functional vascular organoids via simultaneous transcription factor activation of endothelial and mural lineages, Cell Stem Cell (2025), https://doi.org/10.1016/j.stem.2025.05.014

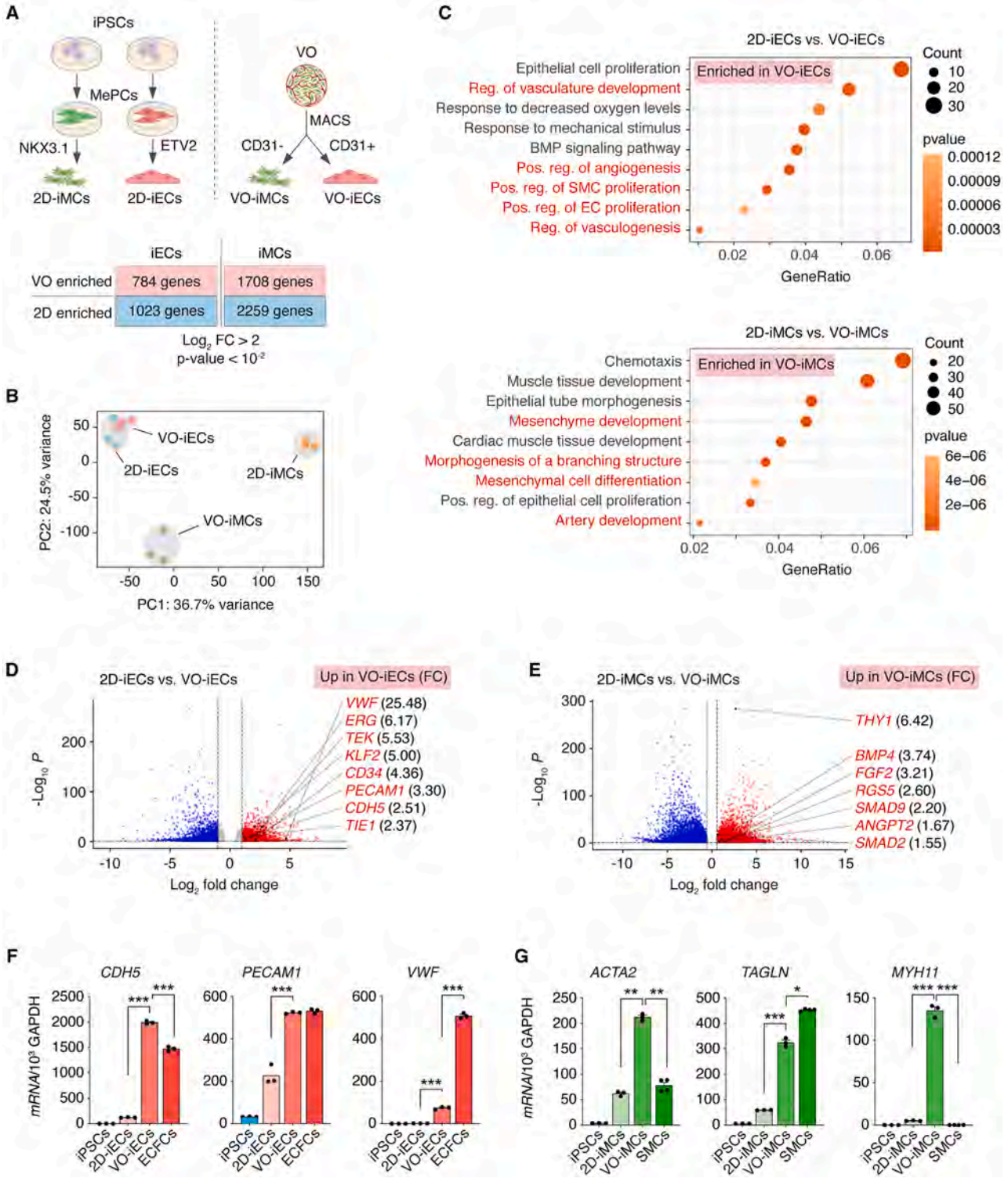

Figure 2. Phenotypic validation and maturation of VO-derived iECs and iMCs

(A) Schematic outlining the generation of VO-derived iECs and iMCs versus 2D monolayer differentiation protocols used as controls. Bulk RNA-seq identified DEGs between 2D-iECs and VO-iECs, as well as 2D-iMCs and VO-iMCs (threshold: $\log_2$ FC > 2; p value < 10^{-2}).

(B) Principal-component analysis (PCA) showing transcriptional similarity of VO-iECs to 2D-iECs and VO-iMCs to 2D-iMCs (n = 3).

(C) Gene Ontology (GO) enrichment analysis revealed upregulation of genes related to vasculature development, angiogenesis, and SMC proliferation in VO-iECs compared with 2D-iECs (top). VO-iMCs showed enrichment of genes associated with mesenchymal development, morphogenesis of branching structures, and artery development (bottom).

(legend continued on next page)

Please cite this article in press as: Gong et al., Rapid generation of functional vascular organoids via simultaneous transcription factor activation of endothelial and mural lineages, Cell Stem Cell (2025), https://doi.org/10.1016/j.stem.2025.05.014

However, DEG analysis between VO and 2D vascular cells revealed significant transcriptional differences associated with maturation. Gene ontology (GO) analysis showed that VO-iECs upregulated genes involved in vasculature development, angiogenesis, vasculogenesis, and smooth muscle cell (SMC) proliferation (Figure 2C). Key endothelial markers—*CDH5*, *VWF*, *ERG*, *TEK*, and *KLF2*—were elevated in VO-iECs versus 2D-iECs by RNA-seq (Figure 2D) and confirmed by qPCR (Figure 2F). Compared with primary ECFCs, VO-iECs expressed similar or higher levels of *CDH5* and *PECAM1*, though *VWF* remained lower, indicating a relatively immature phenotype (Figure 2F).

Similarly, VO-iMCs showed enrichment for genes associated with mature mesenchymal and mural functions, including mesenchyme development, branching morphogenesis, and artery development (Figure 2C). Markers of TGF-β and BMP signaling (e.g., *SMAD9* and *SMAD2*) and angiogenic regulators (*FGF2* and *ANGPT2*) were significantly upregulated (Figure 2E). Contractile genes—*ACTA2*, *TAGLN*, and *MYH11*—were also elevated in VO-iMCs versus 2D-iMCs, as confirmed by qPCR (Figure 2G). Compared with primary SMCs, VO-iMCs showed higher *ACTA2* and *MYH11* expression, likely reflecting the stabilizing role of EC-mural interactions within VOs (Figure 2G).

To contextualize these findings, we compared our TF-based VO (Dox-VO) approach with a chemically induced VO (Chem-VO) protocol adapted from Wimmer et al.[37] While iEC gene expression was largely comparable at day 5, Chem-VOs exhibited markedly lower expression of mural markers such as *ACTA2*, *CNN1*, *TAGLN*, and *MYH11*, indicating reduced mural maturation. Additionally, Chem-VOs contained fewer ECs (~2%) than Dox-VOs at this stage, consistent with the slower EC specification in growth factor-based systems. These results highlight the advantage of the dual TF approach in promoting earlier and more robust vascular specification (Figures S2E–S2I).

Lastly, to evaluate the individual roles of shear stress and co-culture in vascular maturation, we modeled these conditions in 2D. Shear stress alone partially enhanced endothelial maturation, while co-culture with MCs had broader effects on both compartments. The most pronounced maturation occurred when both factors were combined, resembling the integrated cues in VOs. These findings underscore that VO conditions synergistically promote vascular maturation (Figures S2J–S2L).

Together, these results indicate that VO differentiation enhances maturation of both iECs and iMCs.

Further vascular network development upon VO embedding into ECM

A key feature of our VO model is the exclusion of exogenous ECM during early organoid formation. Unlike other VO protocols that require matrix-rich environments such as collagen or Matrigel,[37] our method begins with ECM-free cell aggregates, relying on endogenous ECM deposition over time.

However, we found that subsequent ECM embedding markedly enhanced vascular development. VOs cultured in collagen/Matrigel hydrogels for an additional 5 days without Dox produced mature VOs (mVOs) with expanded, complex vascular networks and diameters nearing 1,000 μm, compared with ~250 μm initially (Figures 3A and 3B). These networks resembled ECM-based VO models and featured dense $CD31^+$ vasculature covered by α-SMA^+ and $MYH11^+$ MCs, with evident lumens by z stack and orthogonal imaging (Figures 3C, 3D, S3A, and S3B; Videos S1 and S2). Basement membrane components, such as collagen type IV, were localized along vessel walls (Figure 3E), and qPCR confirmed *COL4A1* expression in VO-iMCs (Figure 3I), supporting endogenous deposition rather than passive incorporation from the matrix.

To assess vascular maturation after ECM embedding, we dissociated mVOs into single cells and sorted iECs ($CD31^+$, mVO-iECs) and iMCs ($CD31^-$, mVO-iMCs), comparing them with VO-derived cells. qPCR showed upregulation of endothelial markers *PECAM1*, *CDH5*, and *VWF* in mVO-iECs compared with VO-iECs (Figure 3F). Arterial markers (*CXCR4*, *SOX17*, and *NRP1*) were also elevated, while venous markers (*NR2F2*, *NRP2*, and *EPHB4*) were downregulated, indicating a shift toward arterial-like identity. These changes occurred alongside broader endothelial maturation, including higher expression of pan-endothelial genes (Figures 3G and 3H).

In the mural compartment, mVO-iMCs showed increased expression of contractile SMC markers (*ACTA2*, *CNN1*, and *TAGLN*) and reduced expression of pericyte markers (*DES* and *PDE5A*), further supporting vascular maturation and arterialization (Figure 3I).

These results demonstrate that VOs can form extensive, organized vascular networks upon ECM embedding, recapitulating features of ECM-dependent developmental models.

To test whether maturation resulted from ECM embedding rather than extended culture, we compared mVOs (day 10, ECM-embedded) with suspension-cultured VOs of equal duration (VO-D10). mVOs displayed significantly larger diameters (935 ± 78 vs. 340 ± 39 μm) (Figure 3B) and higher expression of EC and MC maturation markers—*PECAM1*, *CDH5*, and *VWF* in iECs, and *ACTA2*, *CNN1*, *TAGLN*, and *MYH11* in iMCs (Figures S3C and S3D)—indicating that ECM embedding, not time alone, drives vascular maturation.

This maturation includes both arterialization of iECs and upregulation of lineage-specific genes across vascular cell types, bringing VOs transcriptionally closer to primary cells and underscoring their physiological relevance.

(D) Volcano plot displaying DEGs in VO-iECs compared with 2D-iECs (threshold: $\log_2FC > 2$).
(E) Volcano plot displaying DEGs in VO-iMCs compared with 2D-iMCs (threshold: $\log_2FC > 1$).
(F) RT-qPCR analysis of endothelial markers *CDH5*, *PECAM1*, and *VWF* in VO-iECs compared with 2D-iECs, showing significant upregulation in VO-iECs ($n = 3$; $p < 0.001$). Human cord blood-derived ECFCs served as primary ECs.
(G) RT-qPCR analysis of MC markers *ACTA2*, *TAGLN*, and *MYH11* in VO-iMCs compared with 2D-iMCs, indicating enhanced expression of SMC-specific markers in VO-iMCs ($n = 3$–4; $^*p$, 0.05, $^{**}p < 0.01$, $^{***}p < 0.001$). Human saphenous vein-derived SMCs served as primary MC control. All PCR data normalized to GAPDH. All data are mean ± SEM (F and G). n are biological replicates (B, F, and G). Statistics are one-way ANOVA with Bonferroni's post-test analysis (F and G). (A) was partially created with BioRender.com.
See also Figure S2.

Please cite this article in press as: Gong et al., Rapid generation of functional vascular organoids via simultaneous transcription factor activation of endothelial and mural lineages, Cell Stem Cell (2025), https://doi.org/10.1016/j.stem.2025.05.014

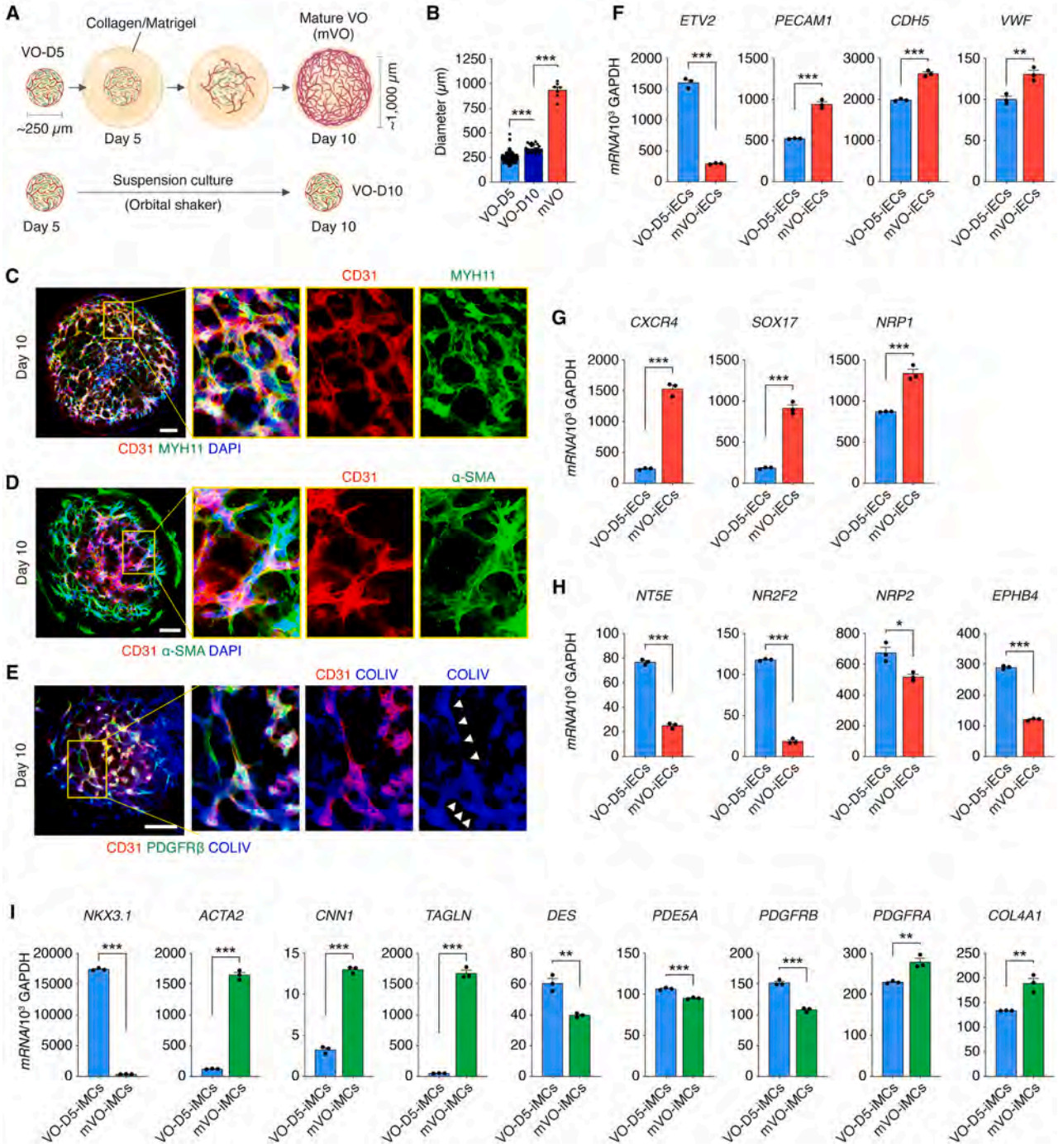

Figure 3. Maturation of VOs upon ECM embedding

(A) Schematic comparing mature vascular organoids (mVOs) generated by embedding VOs in a collagen/Matrigel matrix for 5 days (top) versus VOs maintained in suspension culture for 10 days (VO-D10, bottom).

(B) Quantification of VO diameters. (***$p < 0.001$).

(C–E) Whole-mount immunofluorescence of vascular networks in mVOs on day 5. (C) ECs (CD31$^+$, red) and SMCs (MYH11$^+$, green). (D) ECs (CD31$^+$, red) and α-SMA$^+$ SMCs (green). Nuclei counterstained with DAPI. (E) MCs (PDGFRβ$^+$, green) and basement membrane (Collagen IV$^+$, blue).

(F–H) RT-qPCR of mVO-iECs compared with VO-D5-iECs. (F) Endothelial markers: *ETV2*, *PECAM1*, *CDH5*, and *VWF*. (G) Arterial markers: *CXCR4*, *SOX17*, and *NRP1*. (H) Venous markers: *NT5E*, *NR2F2*, *NRP2*, and *EPHB4*.

(legend continued on next page)

Please cite this article in press as: Gong et al., Rapid generation of functional vascular organoids via simultaneous transcription factor activation of endothelial and mural lineages, Cell Stem Cell (2025), https://doi.org/10.1016/j.stem.2025.05.014

A genetic-footprint-free alternative to generate VOs

An important feature of our TF-mediated differentiation approach is that it relies on the transient expression of ETV2 and NKX3.1, which opens the possibility of using chemically modified mRNA (modRNA) to achieve a genetic-footprint-free protocol. To implement this strategy, we began with unmodified iPSCs and differentiated them into intermediate MePCs over 2 days. We then transfected half of the MePCs with modRNA encoding ETV2 and the other half with modRNA encoding NKX3.1. The transfected populations were combined at a 1:1 ratio, aggregated in 3D using non-adherent culture plates and an orbital shaker, and cultured for 3 additional days (Figure 4A). This modRNA-based method enabled the generation of uniformly sized, footprint-free VOs (modRNA-VOs) within 5 days, comparable in size to Dox-inducible VOs (Figure 4B).

Similar to the Dox-inducible strategy, the modRNA approach enabled simultaneous differentiation of iECs and iMCs within modRNA-VOs. However, despite starting with a 1:1 MePC ratio, the day 5 iEC proportion was lower (20%–30%) than in Dox-VOs (~55%) (Figures 4C and 1D). This discrepancy likely reflects differences in TF expression dynamics: qPCR revealed that ETV2 and NKX3.1 transcript levels in modRNA-VOs peaked early (4 h) and declined rapidly, whereas Dox-VOs maintained higher, sustained expression throughout (Figures S3E and S3F).

Despite this, vascular cell maturation was not impaired in modRNA-VOs, as evidenced by expression of key endothelial and mural markers in iECs and iMCs, respectively (Figures 4D and 4E).

Furthermore, similar to Dox-VOs, modRNA-VOs exhibited robust capacity to mature into vascular networks when embedded in collagen/Matrigel hydrogels. These networks featured $CD31^+$ vessels extensively covered by α-SMA^+ and $MYH11^+$ iMCs, indicating vessel maturation (Figure 4F). This contrasts with earlier stages, where α-SMA expression was more localized and less organized (Figure 1F). The additional 5-day ECM embedding period enabled further mural maturation and structured coverage of endothelial networks.

Shorter TF activation promotes arterial identity

A key difference between the Dox- and modRNA-based methods is the duration of TF expression: Dox enables sustained activation, whereas modRNA yields transient (~24 h) expression. To examine how reduced TF activation impacts VO development and EC identity, we compared the standard 3-day Dox protocol (Dox3-VOs) with a 1-day Dox exposure (Dox1-VOs) during the 3-day culture period (Figure 5A).

There were no significant differences in VO size between Dox1-VOs and Dox3-VOs at day 5 (Figure 5B), and both yielded ~50% $CD31^+$ iECs (Figure 5C). However, flow cytometry revealed distinct iEC compositions. Dox3-VOs harbored heterogeneous endothelial populations, comprising arterial-like ($CD31^+/CXCR4^+$), venous-like ($CD31^+/CXCR4^-/CD73^+$), and other ECs ($CD31^+/CXCR4^-/CD73^-$). To support the arterial identity of $CXCR4^+$ iECs in Dox3-VOs, we sorted $CXCR4^+$ and $CXCR4^-$ subsets and confirmed higher arterial marker expression in the $CXCR4^+$ population by qPCR (Figure S4A). In contrast, Dox1-VOs were predominantly composed of arterial-like iECs ($CD31^+/CXCR4^+$), suggesting enhanced arterialization (Figure 5C). qPCR analysis of sorted iECs further supported these findings. Dox3-VO-iECs showed higher expression of venous markers (*NT5E*, *NRP2*, and *NR2F2*), whereas arterial markers (*CXCR4*, *SOX17*, *NRP1*, and *EFNB2*) were elevated in Dox1-VO-iECs (Figure 5D). Immunofluorescence confirmed EC heterogeneity in Dox3-VOs, showing both $SOX17^+$ arterial-like and $SOX17^-$ non-arterial iECs within vascular structures (Figure 5E).

Interestingly, the emergence of venous-like iECs with prolonged Dox exposure required a 3D VO environment. While the 2D protocol yielded a higher percentage of iECs, it failed to produce venous-like ($CD31^+/CXCR4^-/CD73^+$) iECs (<1%) (Figures S2A and S2B). Expression of venous markers *NT5E*, *NRP2*, and *NR2F2* was also markedly lower in Dox3-2D-iECs compared with Dox3-VO-iECs (Figure S2C). In contrast, Dox1 favored arterial-like iECs in both settings, though arterial marker expression remained higher in Dox1-VOs (Figure S2D).

We also assessed the functional properties of iECs. Dox3-VO-iECs exhibited higher proliferation rates than Dox1-VO-iECs (Figures S4B–S4D). Nonetheless, both populations showed comparable ability to form vascular networks *in vitro* (Figure S4E) and similarly upregulated leukocyte adhesion molecules in response to TNF-α (Figure S4F).

Previous studies have shown that venous ECs possess greater angiogenic potential than arterial ECs. To examine this in VOs, we embedded GFP-labeled Dox1-VOs and Dox3-VOs in fibrin gels and stimulated them with angiogenic factors for 24 h to assess endothelial sprouting (Figure 5F). Quantification revealed significantly more sprouts in Dox3-VOs, indicating robust angiogenic activity. In contrast, Dox1-VOs exhibited fewer sprouts, which increased upon treatment with the NOTCH inhibitor DAPT, whereas Dox3-VOs remained unaffected. These findings support the arterial-like phenotype of Dox1-VO-iECs, marked by reduced sprouting and NOTCH sensitivity.

To assess whether these phenotypic differences translate into functional outcomes *in vivo*, we transplanted Dox1-VOs and Dox3-VOs under the renal capsule of NSG mice (Figure 5G). Both groups exhibited similar engraftment, as shown by bioluminescence tracking of luciferase-labeled iECs over 4 weeks (Figure 5H). However, histological analysis revealed more perfused microvessels in Dox3-VO grafts (Figures 5I and 5J), indicating superior vascular integration. Immunofluorescence confirmed more frequent incorporation of Dox3-iECs into vessel structures, while many iECs in Dox1-VOs remained as isolated, non-incorporated cells (Figure 5K). Dox3-VO grafts also exhibited a mix of arterial-like vessels (α-SMA^+ mural coverage) and venous-like vessels (lacking α-SMA), whereas Dox1-VO grafts were predominantly arterial. Venous-like identity in Dox3-iECs was further supported

(I) RT-qPCR of mVO-iMCs compared with VO-D5-iMCs showing expression of *NKX3.1* and SMC markers (*ACTA2*, *CNN1*, and *TAGLN*), and pericyte markers (*DES* and *PDE5A*). All PCR data normalized to *GAPDH* ($n = 3$; $^*p < 0.05$, $^{**}p < 0.01$, and $^{***}p < 0.001$). Scale bars: 100 μm (C and D) and 200 μm (E).
All data are mean ± SEM (E–H). *n* indicates biological replicates (E–H). Statistics are one-way ANOVA with Bonferroni's post-test analysis (B) and unpaired two-tailed t test (F–I). (A) was partially created with BioRender.com.
See also Figure S3 and Videos S1 and S2.

Please cite this article in press as: Gong et al., Rapid generation of functional vascular organoids via simultaneous transcription factor activation of endothelial and mural lineages, Cell Stem Cell (2025), https://doi.org/10.1016/j.stem.2025.05.014

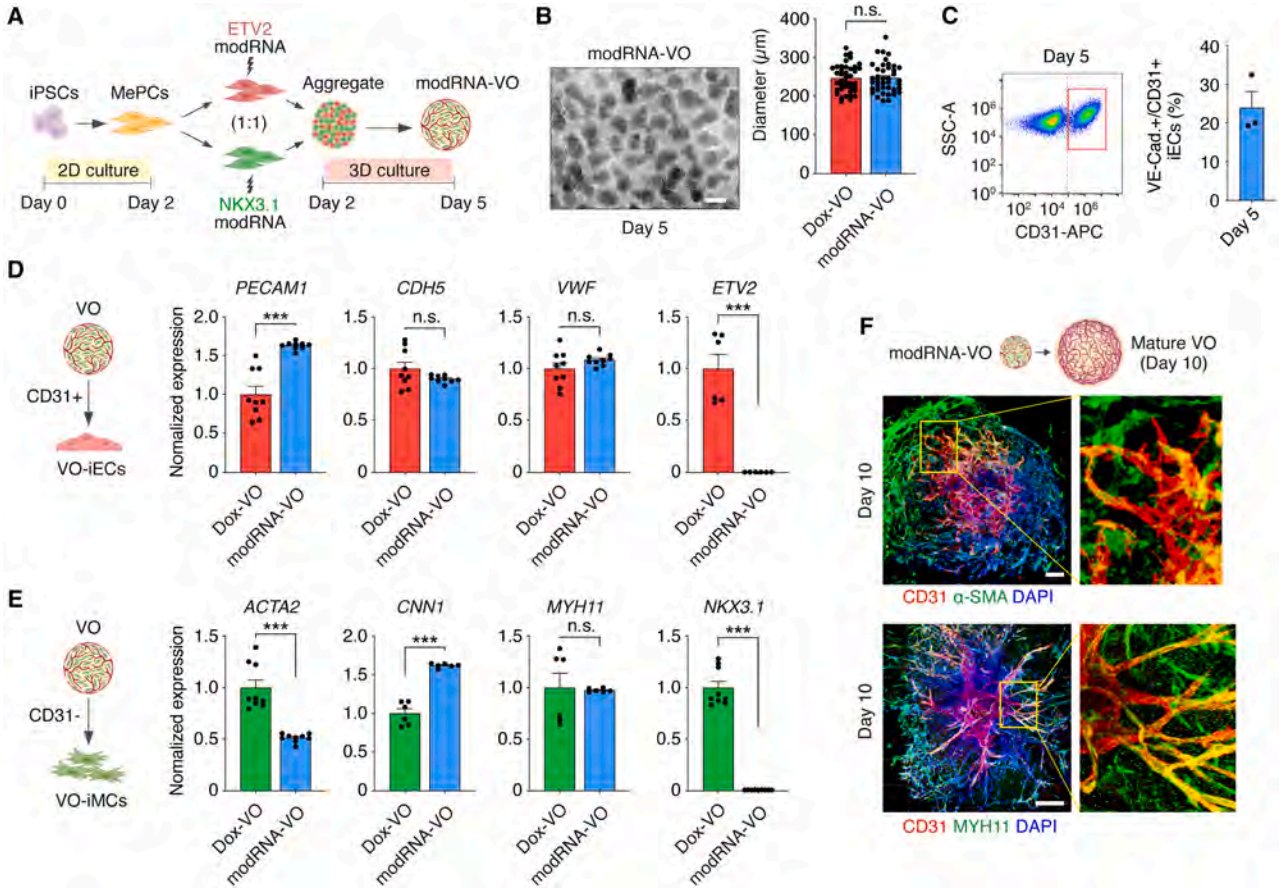

Figure 4. Comparative analysis of doxycycline-induced and modRNA-mediated generation of VOs

(A) Schematic outlining the differentiation of iPSCs into VOs using a modRNA-based method, with MePCs transfected with ETV2 and NKX3.1 modRNA to generate modRNA-VOs.

(B) Bright-field image of modRNA-VOs on day 5 (left) and comparison of VO diameters between Dox-VO and modRNA-VO (right) (n = 40).

(C) Flow cytometry analysis of CD31 expression in modRNA-VOs on day 5 (left) with quantification of CD31$^+$/VE-Cadherin$^+$ iECs (right).

(D) RT-qPCR analysis of *ETV2* and endothelial markers (*PECAM1*, *CDH5*, and *VWF*) in CD31$^+$ iECs isolated from Dox-VOs and modRNA-VOs (n = 6–9; ***p < 0.001).

(E) RT-qPCR analysis of *NKX3.1* and SMC markers (*ACTA2*, *CNN1*, and *MYH11*) in CD31$^-$ iMCs isolated from Dox-VOs and modRNA-VOs (n = 6–9; ***p < 0.001). All PCR data are normalized to *GAPDH*.

(F) Whole-mount immunofluorescence of vascular networks from mature modRNA-VOs embedded in collagen/Matrigel for 5 days showing ECs (CD31$^+$, red) and SMCs (α-SMA$^+$, green; MYH11$^+$, green), with nuclei counterstained by DAPI. Scale bars: 200 μm (B) and 100 μm (F).

All data are mean ± SEM (B–E). n indicates biological replicates (C–E) and individual VOs (B). Statistics are unpaired two-tailed t test (B–E). (A) and (D)–(F) were partially created with BioRender.com.

See also Figure S3.

by nuclear NR2F2 (COUP-TFII) expression in hCD31$^+$ vessels (Figure 5L). These results suggest that the angiogenic, venous-like iECs in Dox3-VOs enhance vascular heterogeneity and integration post-transplantation.

Collectively, these findings suggested that shorter TF activation favors a predominant arterial identity in iECs, while prolonged activation results in a more heterogeneous EC population, including venous-like iECs with greater proliferative, sprouting, and engrafting capacity.

VO cell heterogeneity at single-cell level

To characterize vascular cell heterogeneity in VOs, we performed single-cell RNA sequencing (scRNA-seq) on Dox1-VOs and Dox3-VOs at day 5, and on Dox3-VOs cultured for an additional 7 days without Dox (Dox1-D5, Dox3-D5, and Dox3-D12; Figure 6A). Our goal was to examine how TF activation duration and extended culture influence vascular cell maturation and diversification. Using the 10× Genomics platform, we profiled ~10,000 cells per time point, integrating datasets via Seurat. Thirteen transcriptionally distinct populations were identified based on canonical vascular markers (Figures 6B, 6C, and S5), including four endothelial clusters (#1–4; *CDH5*, *PECAM1*, and *KDR*), five mural clusters (#5–9; *PDGFRB*), and four transcriptionally ambiguous clusters (#10–13), provisionally categorized as "undetermined" (Figures 6B and S5).

Among the endothelial clusters, #1 and #2 showed a clear arterial phenotype, expressing markers such as *EFNB2* and *NRP1* (Figures 6D, 6E, and S6). These cells were enriched in

Please cite this article in press as: Gong et al., Rapid generation of functional vascular organoids via simultaneous transcription factor activation of endothelial and mural lineages, Cell Stem Cell (2025), https://doi.org/10.1016/j.stem.2025.05.014

CellPress

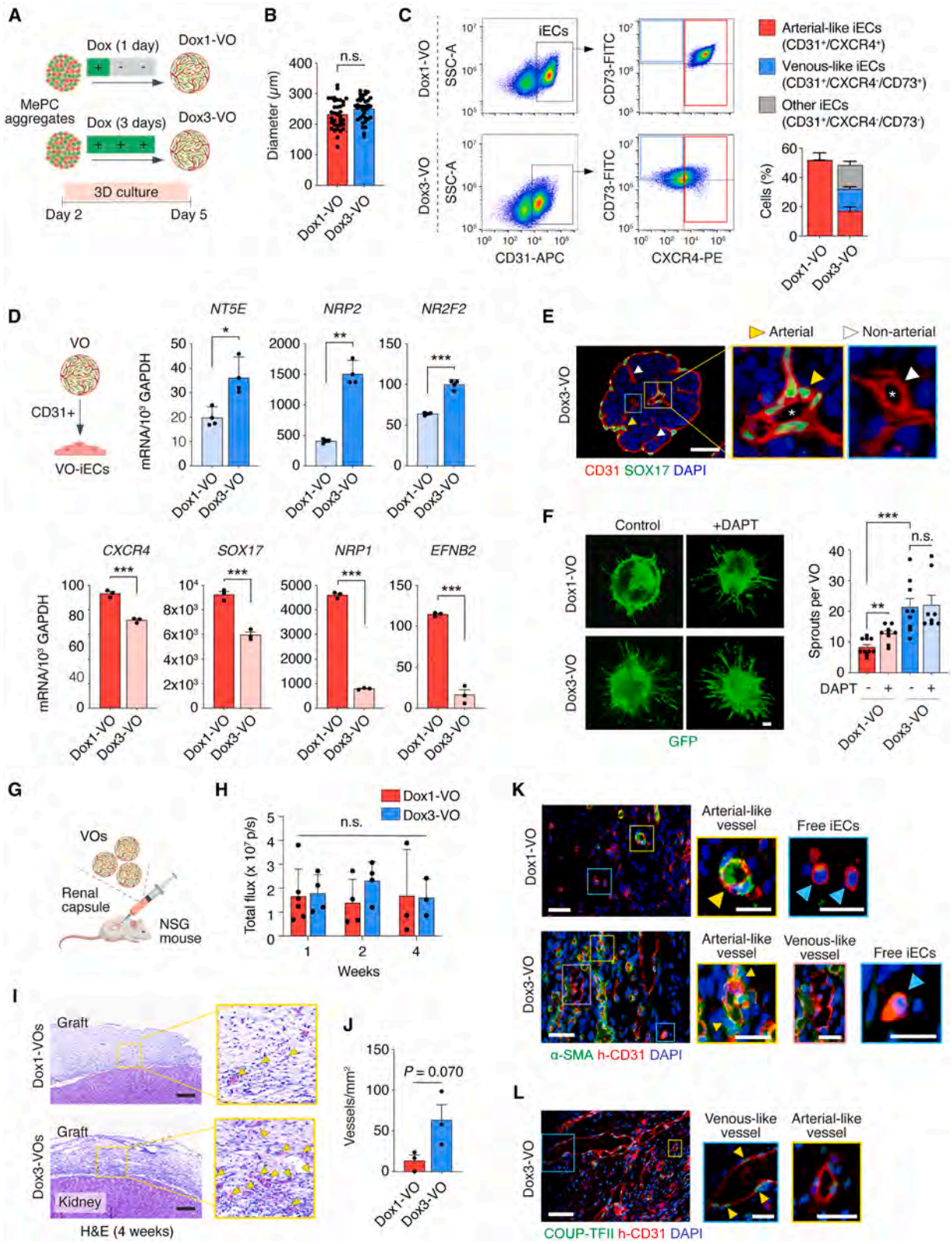

Figure 5. Effect of TF activation duration on iEC identity in VOs

(A) Schematic comparing the differentiation protocols of Dox1-VOs (1-day Dox exposure) and Dox3-VOs (3-day Dox exposure).

(B) Comparison of VO diameters between Dox1-VOs and Dox3-VOs on day 5 ($n > 30$).

(legend continued on next page)

genes linked to arterial specification and development, suggesting advanced arterial differentiation. In contrast, clusters #3 and #4 had less defined arterial identity and exhibited transcriptional profiles associated with angiogenesis and endothelial-to-mesenchymal transition (EndMT), including *ANPEP*, *THY1*, and *ACTA2* (Figures 6D–6F and S6).

Volcano plot analysis revealed distinct transcriptional signatures, with cluster #1 enriched for arterial markers (*NRP1*, *CXCR4*, *HEY1*, *EFNB2*, *DLL4*, *JAG2*, and *SOX17*), while cluster #3 upregulated genes linked to EndMT and TGF-β signaling (Figure 6F). GO term analysis further supported this divergence: cluster #1 was associated with endothelial and arterial development, whereas cluster #3 related to angiogenesis and mesenchymal differentiation (Figures S7A and S7B). Cluster #4 shared similarities with cluster #3 but also expressed cell-cycle markers, indicating a proliferative iEC population (Figures 6B–6E and S6).

To further evaluate the venous identity of iECs observed by flow cytometry and qPCR in Dox3-VOs (Figure 5), we examined whether angiogenic cluster #3 corresponds to a venous-like precursor population. Canonical venous markers (*NT5E*, *NR2F2*, *NRP2*, *EPHB4*, and *APLNR*) were enriched in cluster #3 but also detected in cluster #1, annotated as arterial iECs (Figure S8A). This overlap is consistent with developmental studies showing arterial ECs emerge from venous progenitors via gradual reprogramming, during which venous transcripts persist transiently. The co-expression of venous markers in cluster #1 at day 5 likely represents a transitional state. By day 12, cluster #1 exhibited downregulation of venous markers and upregulation of arterial genes, supporting progressive arterial specification (Figure S8B).

To investigate the developmental trajectory between these iEC populations, we conducted RNA velocity analysis using a PAGA-initialized model. This revealed a directional flow from cluster #3 to cluster #1, consistent with a transition from a venous-like, angiogenic precursor state to a more differentiated arterial phenotype (Figure S8C). Pseudotime analysis supported this view, placing cluster #3 at early and cluster #1 at late pseudotime values (Figure S8C). Additionally, day 5 iECs from Dox3-VOs—representing cluster #3—expressed similar or higher levels of venous markers compared with HUVECs (Figure S8D). These findings support a model in which arterial iECs emerge from angiogenic precursors via progressive downregulation of venous markers and upregulation of arterial genes.

In the MC compartment, we identified four PDGFRB$^+$ clusters: SMCs (cluster #5), pericytes (cluster #6), fibroblasts (cluster #7), and mural progenitor cells (iMPCs; cluster #8) (Figures 6G, 6H, and S9). SMCs were marked by high expression of contractile proteins (*TAGLN* and *ACTA2*), ECM components (*COL1A1*), and low *PDGFRA*, as well as genes linked to oxidative phosphorylation and mitochondrial respiration (Figures S7C and S7D). Pericytes showed lower levels of *TAGLN*, *ACTA2*, and *COL1A1* but higher expression of *PDE5A* and TGF-β receptors (Figures 6G–6I and S9). Both populations expressed *COL4A1* and *FN1*, supporting their perivascular identity (Figure S9).

Cluster #7 was identified as fibroblasts based on high expression of *PDGFRA* and ECM components but low levels of contractile proteins. Cluster #8 represented NKX3.1-expressing iMPCs,[31] while cluster #9 was characterized as proliferating MCs due to elevated cell-cycle marker expression (Figure S9).

To further interpret the transcriptional identity of the undetermined clusters (#10–13), we projected our data onto a recently published multi-organ vascular reference atlas containing transcriptional profiles of fetal, pediatric, and adult endothelial and mural subtypes.[41] This comparison confirmed our annotations of clusters #1–4 and #5–9 as endothelial and mural, respectively (Figure S10). In contrast, clusters #10–13 showed low expression of canonical endothelial and mural markers (Figure S11) and mapped diffusely across the reference, lacking the tight alignment seen for iEC and iMC clusters (Figure S10). Most cells in these clusters aligned with capillary-like endothelial subtypes, which lack strong arterial or venous signatures and are thought to represent immature or transitional states. Based on these findings, we retain the undetermined label in the UMAP but interpret clusters #10–13 as predominantly EC-like populations undergoing early specification or incomplete differentiation.

(C) Flow cytometry analysis of iEC composition in Dox1-VOs and Dox3-VOs on day 5 (left) with quantification of arterial-like (CD31$^+$/CXCR4$^+$), venous-like (CD31$^+$/CXCR4$^-$/CD73$^+$), and other ECs (right) (n = 3).
(D) RT-qPCR analysis of arterial (*CXCR4*, *SOX17*, *NRP1*, and *EFNB2*) and venous (*NT5E*, *NRP2*, and *NR2F2*) markers in CD31$^+$ iECs isolated from Dox1-VOs and Dox3-VOs (n = 3–4; $^*p < 0.05$, $^{**}p < 0.01$, and $^{***}p < 0.001$). All PCR data normalized to *GAPDH*.
(E) Immunofluorescence staining of Dox3-VOs showing arterial-like (SOX17$^+$, yellow arrowheads) and non-arterial (SOX17$^-$, white arrowheads) CD31$^+$ iECs.
(F) Vascular sprouting assay of GFP-labeled (ETV2) Dox1-VOs and Dox3-VOs embedded in fibrin gel, comparing control and DAPT-treated conditions (n = 8–10; $^{**}p < 0.01$ and $^{***}p < 0.001$).
(G) Schematic representation of the renal capsule transplantation model in NSG mice.
(H) Bioluminescence imaging quantification of luciferase-labeled VOs over 4 weeks showing comparable engraftment between Dox1-VOs and Dox3-VOs (n = 3–6).
(I) H&E staining of explanted grafts at 4 weeks. Yellow arrowheads indicate perfused blood vessels containing red blood cells.
(J) Quantification of perfused vessel density at 4 weeks (n = 3).
(K) Immunofluorescence staining of explanted grafts for human CD31 (red), α-SMA (green), and DAPI (blue) to assess vascular architecture and MC association. Arterial-like vessels were defined as small-diameter hCD31$^+$ structures surrounded by α-SMA$^+$ MCs (yellow arrowheads), while venous-like vessels lacked α-SMA coverage and were only observed in Dox3-VO grafts. Free hCD31$^+$ iECs not incorporated into vessel structures (blue arrowhead) were more abundant in Dox1-VO grafts. Insets show representative examples of each category.
(L) Immunofluorescence staining of explanted Dox3-VO grafts for human CD31 (red), NR2F2/COUP-TFII (green), and DAPI (blue) to assess venous endothelial identity. Venous-like vessels were identified by nuclear expression of NR2F2 in hCD31$^+$ ECs (yellow arrowheads). Insets show representative NR2F2$^+$ (venous-like) and NR2F2$^-$ (arterial-like) vessels.
All data are mean ± SEM (B–D, F, H, and J). n indicates biological replicates (C, D, F, H, and J) and individual VOs (B). Statistics are unpaired two-tailed t test (B, D, and J) and one-way ANOVA with Bonferroni's post-test analysis (F and H). (A), (D), and (G) were partially created with BioRender.com.
See also Figure S4.

Please cite this article in press as: Gong et al., Rapid generation of functional vascular organoids via simultaneous transcription factor activation of endothelial and mural lineages, Cell Stem Cell (2025), https://doi.org/10.1016/j.stem.2025.05.014

CellPress

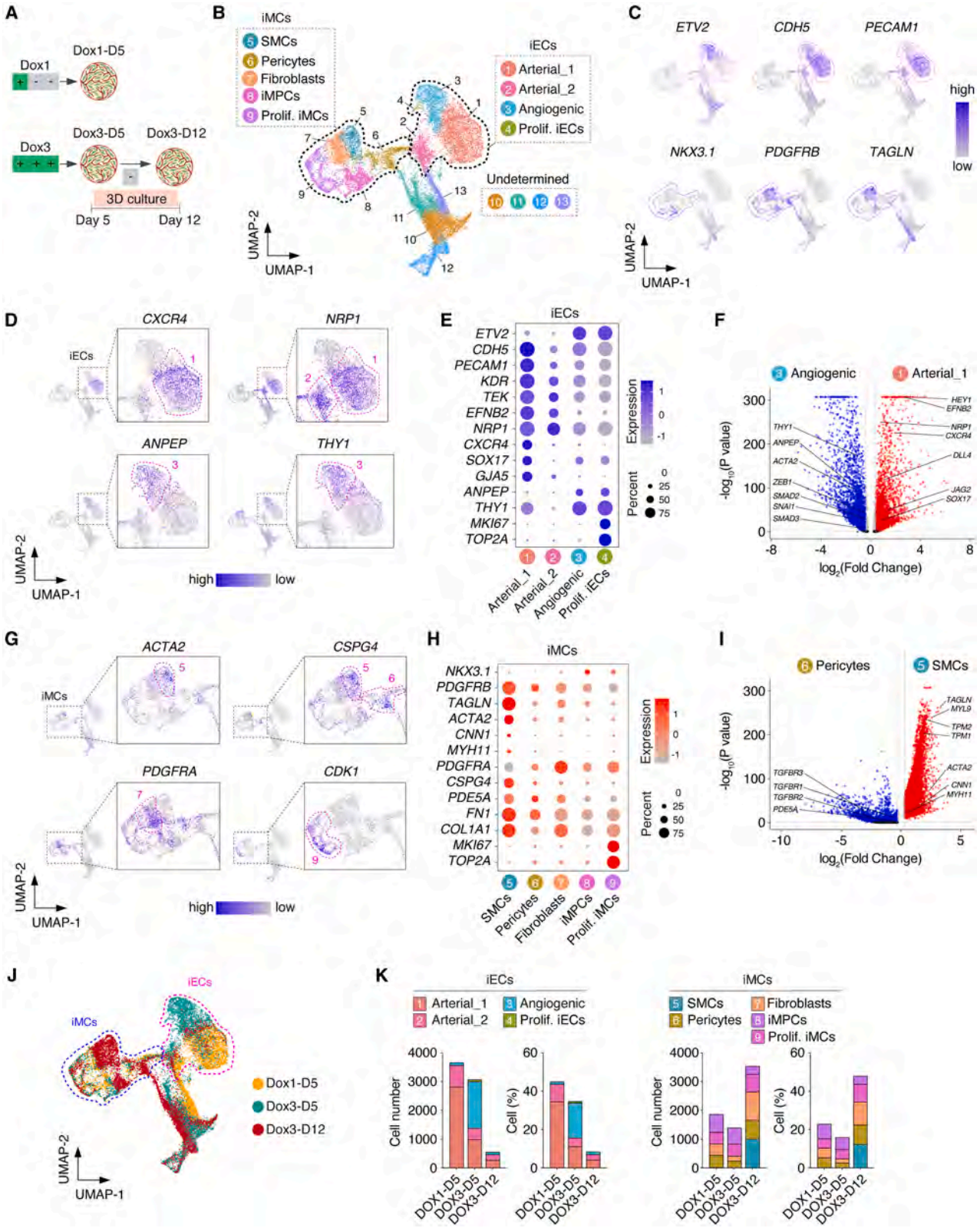

Figure 6. Single-cell RNA sequencing reveals endothelial and MC heterogeneity within VOs

(A) Experimental schematic showing generation of Dox1-D5, Dox3-D5, and Dox3-D12 samples. Dox1-D5 and Dox3-D5 VOs were cultured with doxycycline (Dox) for 1 and 3 days, respectively, while Dox3-D12 VOs were cultured for an additional 7 days without Dox.

(legend continued on next page)

Please cite this article in press as: Gong et al., Rapid generation of functional vascular organoids via simultaneous transcription factor activation of endothelial and mural lineages, Cell Stem Cell (2025), https://doi.org/10.1016/j.stem.2025.05.014

We then evaluated how TF activation duration (Dox1 vs. Dox3) and extended culture (Dox3-D5 vs. Dox3-D12) influenced iEC and iMC populations (Figures 6J and 6K). Shorter activation (Dox1) enriched arterial-like iECs (clusters #1 and #2), while prolonged activation (Dox3) favored angiogenic iECs (cluster #3), aligning with our prior observations of enhanced arterialization in Dox1-VOs and increased sprouting in Dox3-VOs (Figure 5)—reinforcing that TF activation duration impacts iEC fate.

In contrast, MC composition was largely unaffected by TF activation length. Both Dox1 and Dox3 predominantly produced pericytes, fibroblasts, and iMPCs, with few mature SMCs detected at day 5 (Figures 6J and 6K).

Upon extended *in vitro* culture (Dox3-D12), iECs declined from ~50% at Dox3-D5 to <10%, as confirmed by flow cytometry across three VO batches (Figures S8E–S8G). This drop coincided with Dox withdrawal and diminished ETV2 expression. Meanwhile, arterial-like iECs (clusters #1 and #2) increased, and angiogenic iECs (cluster #3) disappeared (Figures 6J and 6K)—indicative of vascular maturation via pruning and arterialization. Concurrently, the mural compartment showed increased mature SMCs, pericytes, and fibroblasts by Dox3-D12 (Figures 6J and 6K). These phenotypic shifts were supported by qPCR showing upregulation of endothelial and mural markers (Figures S8H and S8I).

Together, scRNA-seq analyses demonstrate that (1) VOs capture vascular cell heterogeneity across iEC and iMC lineages, (2) TF activation duration shapes endothelial phenotypes, and (3) extended culture promotes arterialization and MC maturation.

In vivo therapeutic potential of VOs

We previously showed that VOs can engraft into healthy tissues such as the renal capsule and form functional vascular connections with host circulation (Figures 1H–1K and 5G–5L). Building on this, we tested their therapeutic potential in disease models requiring revascularization.

We used a murine hind limb ischemia model in diabetic, immunodeficient nude mice—rendered diabetic with streptozotocin (STZ), as diabetes impairs collateral revascularization.[42,43] After ligating the proximal and deep femoral vessels and excising the intervening segment, we injected 1,000 VOs with luciferase-expressing iECs in 50 μL Matrigel at the ligation site (Figure 7A). For comparison, another group received an equivalent number of iECs and iMCs from 2D protocols as a single-cell suspension in Matrigel.

VO engraftment in ischemic limbs was monitored via bioluminescence imaging on days 1 and 7 (Figure 7B). VOs remained localized at the injection site, with some signal loss during the first week. Nonetheless, VO engraftment was markedly greater than that of single-cell suspensions (Figure 7B). Histological analysis at 2 weeks supported these findings: limbs treated with VOs contained numerous microvessels lined by human $CD31^+$ iECs, whereas vessels in single-cell-treated limbs were largely of mouse origin (Figure 7C).

Most notably, VO treatment significantly improved blood flow recovery in ischemic limbs. Laser Doppler imaging showed ~50% recovery (normalized to the contralateral healthy limb) by 2 weeks (Figure 7D), markedly exceeding the minimal restoration seen with single-cell treatment. VO-treated limbs also exhibited significantly less necrosis than controls or single-cell-treated limbs, which developed severe tissue damage in most cases (Figure 7E). These results demonstrate that VOs effectively engraft, restore perfusion, and prevent necrosis in a diabetic hind limb ischemia model.

We next tested the therapeutic potential of VOs in a pancreatic islet transplantation model. Specifically, we assessed whether VO-mediated revascularization could improve islet engraftment and function. Mouse islets (m-islets), with or without 1,500 VOs, were transplanted under the kidney capsule of STZ-treated diabetic NSG mice (Figure 7F). Groups received 500, 300, or 100 islet equivalents (IEQ) per mouse.

At 500 IEQ, both groups (with and without VOs) became normoglycemic shortly after transplantation, indicating this dose sufficed to correct hyperglycemia (Figure 7G). To better evaluate the VO benefit, we reduced the islet doses to 300 and 100 IEQ—suboptimal levels for normoglycemia restoration. Diabetic NSG mice received either islets alone or islets plus 1,500 VOs. All mice receiving 300 IEQ + VOs and half receiving 100 IEQ + VOs achieved and maintained normoglycemia for up to 100 days. In contrast, only a few mice with 300 IEQ alone and none with 100 IEQ alone reached normoglycemia. Nephrectomy performed 2 days before day 100 led to rapid hyperglycemia, confirming that transplanted islets had maintained glycemic control.

To investigate m-islet-VO interactions, we analyzed kidneys bearing grafts 2 weeks post-transplantation. H&E and IF staining showed INS^+ islets surrounded and infiltrated by perfused vessels, indicating successful vascular integration (Figure 7H). Notably, these vessels were lined by human $CD31^+$ iECs, confirming their VO origin (Figure 7I).

In summary, findings from this second model suggested that co-transplantation with VOs enhances the functional engraftment of pancreatic islets. By promoting revascularization, VOs enabled the use of a reduced number of m-islets to effectively reverse diabetes in mice.

(B) UMAP plot showing 13 distinct cell clusters, including arterial iECs, angiogenic iECs, proliferative iECs, SMCs, pericytes, fibroblasts, mural progenitor cells (iMPCs), and proliferative iMCs.
(C) UMAP feature plots displaying expression of key endothelial (*CDH5* and *PECAM1*) and mural (*PDGFRB* and *TAGLN*) markers across clusters.
(D) Expression of arterial markers (*CXCR4* and *NRP1*) and EndMT markers (*ANPEP* and *THY1*) distinguishing arterial and angiogenic iEC clusters.
(E) Dot plot showing marker expression across iEC clusters, delineating iEC identities.
(F) Volcano plots highlighting DEGs in arterial (Arterial_1) and angiogenic iEC clusters (threshold: $\log_2FC > 1$).
(G) Feature plots for markers (*ACTA2*, *CSPG4*, *PDGFRA*, and *CDK1*), defining SMC, pericyte, fibroblast, and proliferative iMC clusters.
(H) Dot plot of MC markers across iMC clusters.
(I) Volcano plots of pericyte versus SMC gene expression, highlighting distinct markers (threshold: $\log_2FC > 1$).
(J) UMAP of cells by sample type, showing changes in cluster distribution across conditions.
(K) Bar graphs showing cell counts and percentages of iEC and iMC populations across conditions, illustrating shifts in cell composition with prolonged TF activation and extended culture.
See also Figures S5–S11.

Please cite this article in press as: Gong et al., Rapid generation of functional vascular organoids via simultaneous transcription factor activation of endothelial and mural lineages, Cell Stem Cell (2025), https://doi.org/10.1016/j.stem.2025.05.014

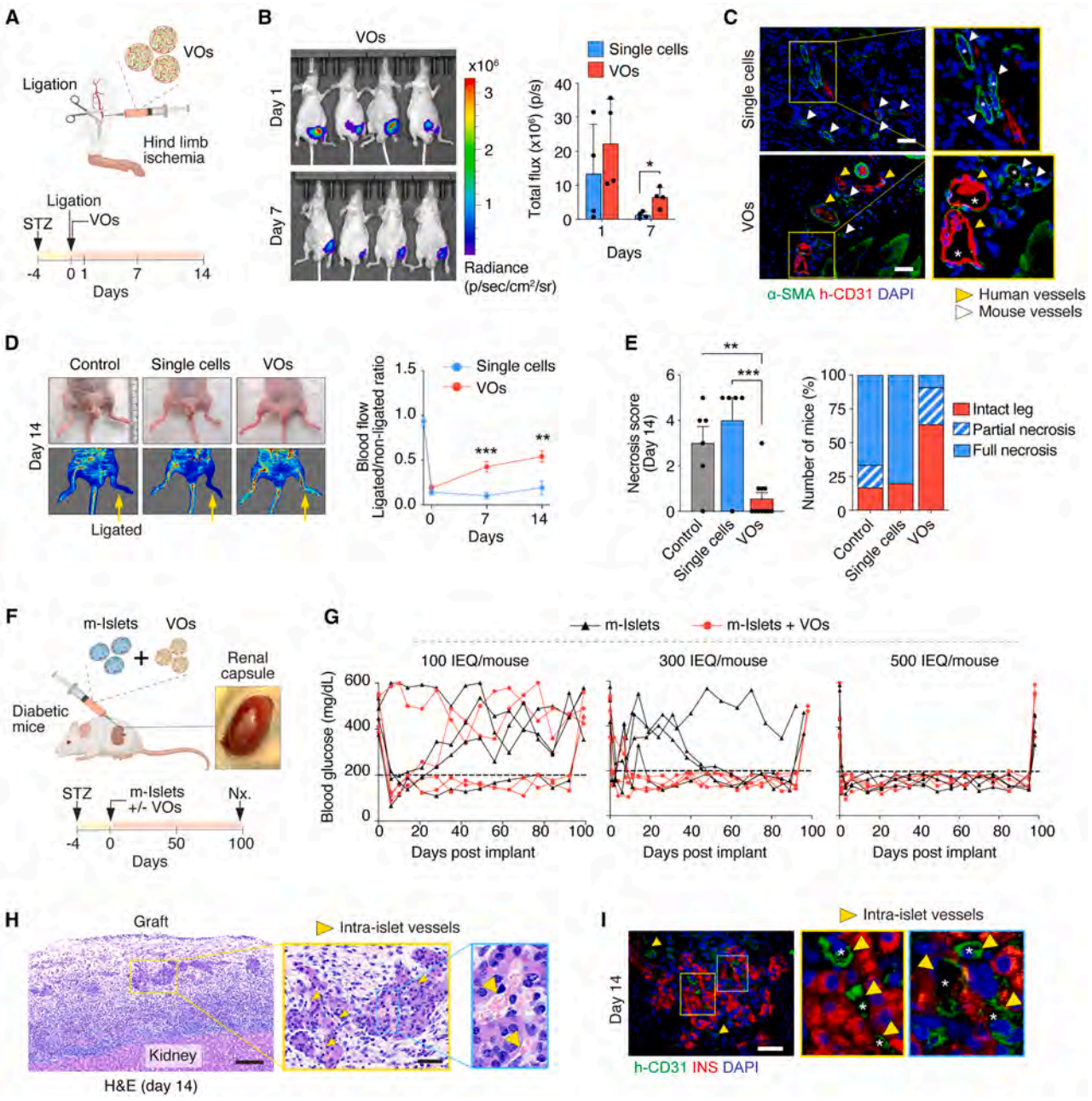

Figure 7. *In vivo* therapeutic potential of VOs

(A) Schematic and timeline of the hind limb ischemia model in immune-deficient nude mice, including diabetes induction with streptozotocin (STZ) and femoral vascular ligation followed by VO transplantation.

(B) Bioluminescent imaging of VO-transplanted mice on days 1 and 7 (left), with quantitative analysis of bioluminescence intensity comparing VOs and single-cell grafts (right) ($n = 4$; $^{*}p < 0.05$).

(C) Immunofluorescence staining of hind limb muscles at day 14, highlighting human-specific CD31^{+} (red) vessels (yellow arrowheads) and mouse vessels (white arrowheads). Vessels are covered by α-SMA^{+} (green) perivascular cells.

(D) Laser Doppler imaging showing blood flow recovery in ischemic limbs over 14 days (left), with quantification of the ligated-to-non-ligated leg blood flow ratio (right) ($n = 6$–12; $^{**}p < 0.01$ and $^{***}p < 0.001$).

(E) Necrosis score on day 14 (left) and necrosis incidence per group (right). Necrosis scoring: 0, no necrosis; 1, toes necrosis; 2, foot necrosis; 3, knee necrosis; 4, femoral necrosis; and 5, whole leg necrosis. Intact leg: necrosis score = 0; partial necrosis: score = 1–2; and full necrosis: score = 3–5 ($n = 6$–12; $^{**}p < 0.01$ and $^{***}p < 0.001$).

(F) Schematic of the kidney capsule transplantation model using diabetic NSG mice. Nx, nephrectomy (removal of the graft-bearing kidney).

(G) Non-fasting blood glucose levels of mice transplanted with mouse islets (m-islets) with or without VOs ($n = 4$) at varying islet equivalent (IEQ) doses.

(H) H&E staining of islet grafts at day 14, with perfused intra-islet vessels indicated (yellow arrowheads).

(legend continued on next page)

Please cite this article in press as: Gong et al., Rapid generation of functional vascular organoids via simultaneous transcription factor activation of endothelial and mural lineages, Cell Stem Cell (2025), https://doi.org/10.1016/j.stem.2025.05.014

DISCUSSION

In this study, we present a streamlined method for generating VOs from iPSCs via orthogonal TF induction using Dox-inducible or modRNA technology. By controlling ETV2 and NKX3.1 expression, we rapidly co-differentiated MePCs into iECs and iMCs, producing uniformly sized 3D VOs with vascular structures in just 5 days. This fast and simplified approach supports both *in vitro* and *in vivo* applications, including disease models of hind limb ischemia and islet transplantation, where VOs promoted revascularization and recovery.

Current VO protocols, including those by Wimmer et al., have advanced *in vitro* modeling of vascular development.[38,44–47] Many involve ECM embedding after initial differentiation but require prolonged culture and multiple steps, affecting scalability and reproducibility.[37] Other approaches, such as MePC incorporation or hanging-drop methods, often use primary cells or complex protocols.[48–50] Our orthogonal TF induction offers an alternative focused on early, precise vascular specification. By co-generating iECs and iMCs within 5 days without early ECM embedding, our method simplifies and scales VO formation.

While our method uses Matrigel during 2D mesodermal induction, 3D aggregate formation proceeds without continuous ECM support. This early independence promotes cell-driven matrix deposition, reducing ECM manipulation during organoid assembly. The self-organizing process also eliminates manual ECM extraction, a complication in other protocols.[37] At later stages, ECM embedding enhances vascular maturation, yielding larger, lumenized vessels. Thus, our protocol supports both ECM-independent and ECM-enhanced phases, balancing scalability with the potential for further maturation in basic and translational studies.

An important feature of our approach is the ability to control iEC and iMC differentiation independently. Existing protocols often favor one lineage due to incompatible culture requirements, with factors such as VEGF promoting iECs while indirectly inducing iMCs via secondary signaling.[1,12] This limits selective manipulation of vascular cell types. In contrast, our orthogonal TF strategy enables simultaneous yet independent generation of iECs and iMCs within the same VO, allowing precise control of cellular composition for mechanistic studies and targeted interventions.

VO-derived cells in our model show functional maturity, with both iECs and iMCs expressing higher levels of vascular-specific genes than in 2D cultures, consistent with enhanced functionality. This aligns with the known role of EC-MC interactions in vascular maturation.[12] VOs formed complex structures, including polarized lumens and perivascular iMCs, within 5 days. These cells also exhibited angiogenic sprouting, ECM remodeling, and host integration, suggesting that their intermediate maturation state may be advantageous for rapid *in vivo* revascularization.

Our system's temporal control over TF activation enables modulation of iEC phenotypes, revealing how transient versus prolonged ETV2 activation affects endothelial identity. Shorter activation (Dox1) promoted arterial-like features, whereas prolonged activation (Dox3) suppressed arterialization and generated a heterogeneous population with angiogenic potential and higher sprouting and engraftment capacity.[51–53] Flow cytometry and qPCR showed upregulation of venous-associated markers and pro-angiogenic function in Dox3-iECs. However, single-cell RNA-seq revealed a more complex picture, with cluster #3 exhibiting pro-angiogenic traits but unclear venous identity.

This discrepancy highlights the difficulty of defining iEC identities based solely on transcriptomic data and points to possible regulatory influences, such as epigenetic or transcriptional mechanisms, underlying the effect of prolonged ETV2 activation on arterial fate. Whether the venous-like traits seen by FACS and qPCR are functionally linked to the observed pro-angiogenic behavior remains unclear. Further studies are needed to clarify this relationship, which could inform strategies to fine-tune endothelial properties for therapeutic use.[29,53]

The overlap of venous and arterial marker expression in our iEC clusters reflects a known developmental trajectory in which arterial fate emerges from venous progenitors. In mammalian embryos, arterial ECs derive from venous ECs via transcriptional reprogramming and spatial reorganization,[54] regulated by flow and Notch signaling in contexts such as the yolk sac and retina.[53,55] Zebrafish imaging has shown venous tip cells contributing retrogradely to arterial vessels.[53] Single-cell studies of human iPSC-derived ECs also reveal arterial cells arising from venous-like intermediates marked by *APLNR* and *NR2F2*, with enhanced angiogenic potential.[29] These data support our interpretation that cluster #3 in Dox3-VOs represents a venous-like precursor transitioning to arterial identity, as evidenced by transcriptional maturation, loss of venous markers, and RNA velocity analysis. Collectively, these findings underscore that venous identity is a dynamic, permissive state along the arterial specification continuum—one that our VO model appears to recapitulate.

While our study focused on VOs, this TF induction system may extend to vascularizing other organoid models, where the lack of integrated vasculature remains a major limitation.[56,57] Incorporating mature vascular cells into organoids often leads to cell segregation, limiting intermingling between cell types.[58] In contrast, orthogonal TF induction enables simultaneous differentiation of parenchymal and vascular cell types, potentially improving integration. Engineered iPSCs with TF switches could be embedded into developing organoids to trigger vascular differentiation upon activation, acting as a "Trojan horse" to deliver vascular cells *in situ*. This strategy could be adapted to organoid systems such as liver, kidney, and brain, where vascularization is essential.[59–63]

Our study also demonstrates the use of modRNA to generate VOs, providing a footprint-free alternative for contexts where permanent genomic integration is undesirable.[64] Because ETV2 and NKX3.1 require only transient expression to guide MePC differentiation, modRNA enables an efficient, short-term

(I) Immunofluorescence staining of grafts on day 14 showing insulin-positive (INS^+, red) islets and human $CD31^+$ iECs (green), with intra-islet vessels indicated (yellow arrowheads). Scale bars: 50 μm (C, H right, I) and 200 μm (H left).

All data are mean ± SEM (B, D, and E). *n* indicates biological replicates (B, D, E, and G). Statistics are one-way ANOVA with Bonferroni's post-test analysis (B, D, and E). (A) and (F) were partially created with BioRender.com.

expression system that does not integrate into the genome, offering flexibility across diverse iPSC lines. Although modRNA requires an additional transfection step, advances in high-throughput electroporation and clinical-grade reagents may facilitate scalable, translational VO production.[65,66]

Together, these features position our VO platform as a versatile tool for translational applications. *In vivo*, VOs integrated with host vasculature, revascularized ischemic tissues, and supported pancreatic islet transplantation—demonstrating utility in tissue repair. While VO-derived vessels were robustly incorporated, whether iECs acquire tissue-specific phenotypes remains unknown. Further studies are needed to evaluate long-term efficacy and scalability in clinically relevant models, including strategies using autologous or hypoimmunogenic iPSCs for broader therapeutic applicability.[67,68]

In summary, VOs represent a versatile tool with wide-ranging applications in regenerative medicine, disease modeling, and basic vascular biology. The potential for rapid, efficient, and controlled vascular differentiation makes this TF-based approach to generating VOs a promising avenue for addressing critical needs in vascularized tissue engineering and therapeutic applications.

Limitations of the study

Our VO system uses synchronized Dox-dependent activation of TFs to induce both endothelial and MC differentiation, limiting independent modulation of each compartment. Future refinements using orthogonal induction systems or combining Dox with modRNA may offer more flexibility.[69–71] The absence of perfusion in our suspension culture precludes shear stress, a key regulator of endothelial maturation.[72] Incorporating VOs into perfusable systems could enhance physiological relevance.[73,74] Additionally, whether iECs acquire tissue-specific phenotypes post-engraftment remains to be evaluated.

RESOURCE AVAILABILITY

Lead contact

Further information and requests for resources and reagents should be directed to and will be fulfilled by the lead contact, Dr. Juan Melero-Martin (juan.meleromartin@childrens.harvard.edu).

Materials availability

Cells and plasmids generated in this study can be shared by the lead contact upon request. This study did not generate new unique mouse lines.

Data and code availability

- The RNA-seq and single-cell RNA-seq datasets generated and/or analyzed during this study have been deposited in the Gene Expression Omnibus (GEO) under accession number (GEO: GSE281002) and are publicly available as of the date of publication.
- Microscopy data reported in this paper will be shared by the lead contact upon request.
- This paper does not report original code.
- Any additional information required to reanalyze the data reported in this paper is available from the lead contact upon request.

ACKNOWLEDGMENTS

Some illustrations were partially created with BioRender.com. This work was supported by grants from the National Institutes of Health (R01HL128452 and R01HL172968 to J.M.M.-M. and R01HL151450 to J.M.M.-M. and W.T.P.), the Breakthrough T1D Foundation (2-SRA-2023-1314-S-B to J.M.M.-M.), and the Beijing Natural Science Foundation and Beijing Nova Program (JQ23029, 20220484100, and 20230484448 to K.W.).

AUTHOR CONTRIBUTIONS

L.G., K.W., and J.M.M.-M. conceived and designed the project. L.G., U.L., A. C.L., X.L., X.W., D.C., W.T.P., R.-Z.L., M.M., and K.W. performed the experimental work. Y. Zhang performed single-cell transcriptional studies. Y. Zhang, Y. Zhu, and K.C. performed bioinformatical analyses. All authors discussed and analyzed the data and edited the results. L.G. and J.M.M.-M. wrote the manuscript with inputs from all the co-authors.

DECLARATION OF INTERESTS

U.L., K.W., and J.M.M.-M. are inventors on a patent application (Methods of Making and Using iPSC-Derived Mural Progenitor Cells via NKX3.1 Activation; patent number: WO 2025/080915; date of filing: October 11, 2024; filing jurisdiction: PCT [International Application No. PCT/US2024/050882]), filed by the Children's Medical Center Corporation, related to this work.

STAR★METHODS

Detailed methods are provided in the online version of this paper and include the following:

- KEY RESOURCES TABLE
- EXPERIMENTAL MODEL AND STUDY PARTICIPANT DETAILS
  - Animals
  - Cell lines
- METHOD DETAILS
  - Generation of doxycycline-inducible ETV2 and NKX3.1 iPSC lines
  - Generation of vascular organoids
  - VO embedding in collagen/Matrigel matrix
  - Isolation of iECs and iMCs from VOs
  - Quantitative reverse transcription PCR
  - Flow cytometry
  - Immunofluorescence staining
  - Sprouting assay
  - Tube formation assay
  - Leukocyte adhesion molecule assay
  - Animal experiments
  - Bulk RNA sequencing
  - Single-cell RNA sequencing
  - Microscopy
- QUANTIFICATION AND STATISTICAL ANALYSIS

SUPPLEMENTAL INFORMATION

Supplemental information can be found online at https://doi.org/10.1016/j.stem.2025.05.014.

Received: November 11, 2024
Revised: April 10, 2025
Accepted: May 26, 2025

REFERENCES

1. Augustin, H.G., and Koh, G.Y. (2024). A systems view of the vascular endothelium in health and disease. Cell *187*, 4833–4858. https://doi.org/10.1016/j.cell.2024.07.012.
2. Herbert, S.P., and Stainier, D.Y.R. (2011). Molecular control of endothelial cell behaviour during blood vessel morphogenesis. Nat. Rev. Mol. Cell Biol. *12*, 551–564. https://doi.org/10.1038/nrm3176.
3. Cleaver, O., and Melton, D.A. (2003). Endothelial signaling during development. Nat. Med. *9*, 661–668. https://doi.org/10.1038/nm0603-661.

4. Ramasamy, S.K., Kusumbe, A.P., and Adams, R.H. (2015). Regulation of tissue morphogenesis by endothelial cell-derived signals. Trends Cell Biol. *25*, 148–157. https://doi.org/10.1016/j.tcb.2014.11.007.

5. Bautch, V.L. (2011). Stem cells and the vasculature. Nat. Med. *17*, 1437–1443. https://doi.org/10.1038/nm.2539.

6. Eming, S.A., Martin, P., and Tomic-Canic, M. (2014). Wound repair and regeneration: Mechanisms, signaling, and translation. Sci. Transl. Med. *6*, 265sr6. https://doi.org/10.1126/scitranslmed.3009337.

7. Rocha, S.F., and Adams, R.H. (2009). Molecular differentiation and specialization of vascular beds. Angiogenesis *12*, 139–147. https://doi.org/10.1007/s10456-009-9132-x.

8. Rafii, S., Butler, J.M., and Ding, B.-S. (2016). Angiocrine functions of organ-specific endothelial cells. Nature *529*, 316–325. https://doi.org/10.1038/nature17040.

9. Augustin, H.G., and Koh, G.Y. (2017). Organotypic vasculature: From descriptive heterogeneity to functional pathophysiology. Science *357*, eaal2379. https://doi.org/10.1126/science.aal2379.

10. Potente, M., Gerhardt, H., and Carmeliet, P. (2011). Basic and Therapeutic Aspects of Angiogenesis. Cell *146*, 873–887. https://doi.org/10.1016/j.cell.2011.08.039.

11. Carmeliet, P., and Jain, R.K. (2011). Molecular mechanisms and clinical applications of angiogenesis. Nature *473*, 298–307. https://doi.org/10.1038/nature10144.

12. Jain, R.K. (2003). Molecular regulation of vessel maturation. Nat. Med. *9*, 685–693. https://doi.org/10.1038/nm0603-685.

13. Gaengel, K., Genové, G., Armulik, A., and Betsholtz, C. (2009). Endothelial-Mural Cell Signaling in Vascular Development and Angiogenesis. Arterioscler. Thromb. Vasc. Biol. *29*, 630–638. https://doi.org/10.1161/ATVBAHA.107.161521.

14. Wang, K., Lin, R.-Z., and Melero-Martin, J.M. (2019). Bioengineering human vascular networks: trends and directions in endothelial and perivascular cell sources. Cell. Mol. Life Sci. *76*, 421–439. https://doi.org/10.1007/s00018-018-2939-0.

15. Melero-Martin, J.M. (2022). Human Endothelial Colony-Forming Cells. Cold Spring Harb. Perspect. Med. *12*, a041154. https://doi.org/10.1101/cshperspect.a041154.

16. Melero-Martin, J.M., De Obaldia, M.E.D., Kang, S.-Y., Khan, Z.A., Yuan, L., Oettgen, P., and Bischoff, J. (2008). Engineering Robust and Functional Vascular Networks In Vivo With Human Adult and Cord Blood–Derived Progenitor Cells. Circ. Res. *103*, 194–202. https://doi.org/10.1161/CIRCRESAHA.108.178590.

17. Au, P., Tam, J., Fukumura, D., and Jain, R.K. (2008). Bone marrow–derived mesenchymal stem cells facilitate engineering of long-lasting functional vasculature. Blood *111*, 4551–4558. https://doi.org/10.1182/blood-2007-10-118273.

18. Crisan, M., Yap, S., Casteilla, L., Chen, C.-W., Corselli, M., Park, T.S., Andriolo, G., Sun, B., Zheng, B., Zhang, L., et al. (2008). A Perivascular Origin for Mesenchymal Stem Cells in Multiple Human Organs. Cell Stem Cell *3*, 301–313. https://doi.org/10.1016/j.stem.2008.07.003.

19. Ingram, D.A., Mead, L.E., Tanaka, H., Meade, V., Fenoglio, A., Mortell, K., Pollok, K., Ferkowicz, M.J., Gilley, D., and Yoder, M.C. (2004). Identification of a novel hierarchy of endothelial progenitor cells using human peripheral and umbilical cord blood. Blood *104*, 2752–2760. https://doi.org/10.1182/blood-2004-04-1396.

20. Galipeau, J., and Sensébé, L. (2018). Mesenchymal Stromal Cells: Clinical Challenges and Therapeutic Opportunities. Cell Stem Cell *22*, 824–833. https://doi.org/10.1016/j.stem.2018.05.004.

21. Takahashi, K., Tanabe, K., Ohnuki, M., Narita, M., Ichisaka, T., Tomoda, K., and Yamanaka, S. (2007). Induction of Pluripotent Stem Cells from Adult Human Fibroblasts by Defined Factors. Cell *131*, 861–872. https://doi.org/10.1016/j.cell.2007.11.019.

22. Park, I.-H., Zhao, R., West, J.A., Yabuuchi, A., Huo, H., Ince, T.A., Lerou, P.H., Lensch, M.W., and Daley, G.Q. (2008). Reprogramming of human somatic cells to pluripotency with defined factors. Nature *451*, 141–146. https://doi.org/10.1038/nature06534.

23. Lin, Y., Gil, C.-H., and Yoder, M.C. (2017). Differentiation, Evaluation, and Application of Human Induced Pluripotent Stem Cell–Derived Endothelial Cells. Arterioscler. Thromb. Vasc. Biol. *37*, 2014–2025. https://doi.org/10.1161/ATVBAHA.117.309962.

24. Orlova, V.V., van den Hil, F.E., Petrus-Reurer, S., Drabsch, Y., ten Dijke, P., and Mummery, C.L. (2014). Generation, expansion and functional analysis of endothelial cells and pericytes derived from human pluripotent stem cells. Nat. Protoc. *9*, 1514–1531. https://doi.org/10.1038/nprot.2014.102.

25. Cheung, C., Bernardo, A.S., Trotter, M.W.B., Pedersen, R.A., and Sinha, S. (2012). Generation of human vascular smooth muscle subtypes provides insight into embryological origin-dependent disease susceptibility. Nat. Biotechnol. *30*, 165–173. https://doi.org/10.1038/nbt.2107.

26. Trounson, A., and DeWitt, N.D. (2016). Pluripotent stem cells progressing to the clinic. Nat. Rev. Mol. Cell Biol. *17*, 194–200. https://doi.org/10.1038/nrm.2016.10.

27. Cerneckis, J., Cai, H., and Shi, Y. (2024). Induced pluripotent stem cells (iPSCs): molecular mechanisms of induction and applications. Signal Transduct. Target. Ther. *9*, 112. https://doi.org/10.1038/s41392-024-01809-0.

28. Patsch, C., Challet-Meylan, L., Thoma, E.C., Urich, E., Heckel, T., O'Sullivan, J.F., Grainger, S.J., Kapp, F.G., Sun, L., Christensen, K., et al. (2015). Generation of vascular endothelial and smooth muscle cells from human pluripotent stem cells. Nat. Cell Biol. *17*, 994–1003. https://doi.org/10.1038/ncb3205.

29. Ang, L.T., Nguyen, A.T., Liu, K.J., Chen, A., Xiong, X., Curtis, M., Martin, R.M., Raftry, B.C., Ng, C.Y., Vogel, U., et al. (2022). Generating human artery and vein cells from pluripotent stem cells highlights the arterial tropism of Nipah and Hendra viruses. Cell *185*, 2523–2541.e30. https://doi.org/10.1016/j.cell.2022.05.024.

30. Wang, K., Lin, R.-Z., Hong, X., Ng, A.H., Lee, C.N., Neumeyer, J., Wang, G., Wang, X., Ma, M., Pu, W.T., et al. (2020). Robust differentiation of human pluripotent stem cells into endothelial cells via temporal modulation of ETV2 with modified mRNA. Sci. Adv. *6*, eaba7606. https://doi.org/10.1126/sciadv.aba7606.

31. Lee, U., Zhang, Y., Zhu, Y., Luo, A.C., Gong, L., Tremmel, D.M., Kim, Y., Villarreal, V.S., Wang, X., Lin, R.-Z., et al. (2024). Robust differentiation of human pluripotent stem cells into mural progenitor cells via transient activation of NKX3.1. Nat. Commun. *15*, 8392. https://doi.org/10.1038/s41467-024-52678-8.

32. Pan, Z., Yao, Q., Kong, W., Ma, X., Tian, L., Zhao, Y., Zhu, S., Chen, S., Sun, M., Liu, J., et al. (2025). Generation of iPSC-derived human venous endothelial cells for the modeling of vascular malformations and drug discovery. Cell Stem Cell *32*, 227–245.e9. https://doi.org/10.1016/j.stem.2024.10.015.

33. Elcheva, I., Brok-Volchanskaya, V., Kumar, A., Liu, P., Lee, J.-H., Tong, L., Vodyanik, M., Swanson, S., Stewart, R., Kyba, M., et al. (2014). Direct induction of haematoendothelial programs in human pluripotent stem cells by transcriptional regulators. Nat. Commun. *5*, 4372. https://doi.org/10.1038/ncomms5372.

34. Ginsberg, M., James, D., Ding, B.-S., Nolan, D., Geng, F., Butler, J.M., Schachterle, W., Pulijaal, V.R., Mathew, S., Chasen, S.T., et al. (2012). Efficient Direct Reprogramming of Mature Amniotic Cells into Endothelial Cells by ETS Factors and TGFβ Suppression. Cell *151*, 559–575. https://doi.org/10.1016/j.cell.2012.09.032.

35. Armulik, A., Abramsson, A., and Betsholtz, C. (2005). Endothelial/Pericyte Interactions. Circ. Res. *97*, 512–523. https://doi.org/10.1161/01.RES.0000182903.16652.d7.

36. Levenberg, S., Golub, J.S., Amit, M., Itskovitz-Eldor, J., and Langer, R. (2002). Endothelial cells derived from human embryonic stem cells. Proc. Natl. Acad. Sci. USA *99*, 4391–4396. https://doi.org/10.1073/pnas.032074999.

37. Wimmer, R.A., Leopoldi, A., Aichinger, M., Kerjaschki, D., and Penninger, J.M. (2019). Generation of blood vessel organoids from human pluripotent

stem cells. Nat. Protoc. *14*, 3082–3100. https://doi.org/10.1038/s41596-019-0213-z.

38. Wimmer, R.A., Leopoldi, A., Aichinger, M., Wick, N., Hantusch, B., Novatchkova, M., Taubenschmid, J., Hämmerle, M., Esk, C., Bagley, J. A., et al. (2019). Human blood vessel organoids as a model of diabetic vasculopathy. Nature *565*, 505–510. https://doi.org/10.1038/s41586-018-0858-8.

39. Romeo, S.G., Secco, I., Schneider, E., Reumiller, C.M., Santos, C.X.C., Zoccarato, A., Musale, V., Pooni, A., Yin, X., Theofilatos, K., et al. (2023). Human blood vessel organoids reveal a critical role for CTGF in maintaining microvascular integrity. Nat. Commun. *14*, 5552. https://doi.org/10.1038/s41467-023-41326-2.

40. Luo, A.C., Wang, J., Wang, K., Zhu, Y., Gong, L., Lee, U., Li, X., Tremmel, D.M., Lin, R.-Z., Ingber, D.E., et al. (2024). A streamlined method to generate endothelial cells from human pluripotent stem cells via transient doxycycline-inducible ETV2 activation. Angiogenesis *27*, 779–795. https://doi.org/10.1007/s10456-024-09937-5.

41. Barnett, S.N., Cujba, A.-M., Yang, L., Maceiras, A.R., Li, S., Kedlian, V.R., Pett, J.P., Polanski, K., Miranda, A.M.A., Xu, C., et al. (2024). An organotypic atlas of human vascular cells. Nat. Med. *30*, 3468–3481. https://doi.org/10.1038/s41591-024-03376-x.

42. Kolluru, G.K., Bir, S.C., and Kevil, C.G. (2012). Endothelial Dysfunction and Diabetes: Effects on Angiogenesis, Vascular Remodeling, and Wound Healing. Int. J. Vasc. Med. *2012*, 918267. https://doi.org/10.1155/2012/918267.

43. Abacı, A., Oğuzhan, A., Kahraman, S., Eryol, N.K., Ünal, S., Arınç, H., and Ergin, A. (1999). Effect of Diabetes Mellitus on Formation of Coronary Collateral Vessels. Circulation *99*, 2239–2242. https://doi.org/10.1161/01.cir.99.17.2239.

44. Naderi-Meshkin, H., Wahyu Setyaningsih, W.A.W., Yacoub, A., Carney, G., Cornelius, V.A., Nelson, C.-A., Kelaini, S., Donaghy, C., Dunne, P.D., Amirkhah, R., et al. (2024). Unveiling impaired vascular function and cellular heterogeneity in diabetic donor-derived vascular organoids. Stem Cells *42*, 791–808. https://doi.org/10.1093/stmcls/sxae043.

45. Quan, Y., Hu, M., Jiang, J., Jin, P., Fan, J., Li, M., Fan, X., Gong, Y., Yang, Y., and Wang, Y. (2023). VGLL4 promotes vascular endothelium specification via TEAD1 in the vascular organoids and human pluripotent stem cells-derived endothelium model. Cell. Mol. Life Sci. *80*, 215. https://doi.org/10.1007/s00018-023-04858-w.

46. Meijer, E.M., Koch, S.E., van Dijk, C.G.M., Maas, R.G.C., Chrifi, I., Szymczyk, W., Besseling, P.J., Pomp, L., Koomen, V.J.C.H., Buikema, J.W., et al. (2023). 3D Human iPSC Blood Vessel Organoids as a Source of Flow-Adaptive Vascular Cells for Creating a Human-Relevant 3D-Scaffold Based Macrovessel Model. Adv. Biol. (Weinh) *7*, e2200137. https://doi.org/10.1002/adbi.202200137.

47. Ahn, Y., An, J.-H., Yang, H.-J., Lee, W.-J., Lee, S.-H., Park, Y.-H., Lee, J.-H., Lee, H.J., Lee, S.H., and Kim, S.-U. (2024). Blood vessel organoids generated by base editing and harboring single nucleotide variation in Notch3 effectively recapitulate CADASIL-related pathogenesis. Mol. Neurobiol. *61*, 9171–9183. https://doi.org/10.1007/s12035-024-04141-4.

48. Wörsdörfer, P., Dalda, N., Kern, A., Krüger, S., Wagner, N., Kwok, C.K., Henke, E., and Ergün, S. (2019). Generation of complex human organoid models including vascular networks by incorporation of mesodermal progenitor cells. Sci. Rep. *9*, 15663. https://doi.org/10.1038/s41598-019-52204-7.

49. Schmidt, S., Alt, Y., Deoghare, N., Krüger, S., Kern, A., Rockel, A.F., Wagner, N., Ergün, S., and Wörsdörfer, P. (2022). A Blood Vessel Organoid Model Recapitulating Aspects of Vasculogenesis, Angiogenesis and Vessel Wall Maturation. Organoids *1*, 41–53. https://doi.org/10.3390/organoids1010005.

50. Markou, M., Kouroupis, D., Badounas, F., Katsouras, A., Kyrkou, A., Fotsis, T., Murphy, C., and Bagli, E. (2020). Tissue Engineering Using Vascular Organoids From Human Pluripotent Stem Cell Derived Mural Cell Phenotypes. Front. Bioeng. Biotechnol. *8*, 278. https://doi.org/10.3389/fbioe.2020.00278.

51. Trimm, E., and Red-Horse, K. (2022). Vascular endothelial cell development and diversity. Nat. Rev. Cardiol. *20*, 1–14. https://doi.org/10.1038/s41569-022-00770-1.

52. Luo, W., Garcia-Gonzalez, I., Fernández-Chacón, M., Casquero-Garcia, V., Sanchez-Muñoz, M.S., Mühleder, S., Garcia-Ortega, L., Andrade, J., Potente, M., and Benedito, R. (2021). Arterialization requires the timely suppression of cell growth. Nature *589*, 437–441. https://doi.org/10.1038/s41586-020-3018-x.

53. Xu, C., Hasan, S.S., Schmidt, I., Rocha, S.F., Pitulescu, M.E., Bussmann, J., Meyen, D., Raz, E., Adams, R.H., and Siekmann, A.F. (2014). Arteries are formed by vein-derived endothelial tip cells. Nat. Commun. *5*, 5758. https://doi.org/10.1038/ncomms6758.

54. Red-Horse, K., and Siekmann, A.F. (2019). Veins and Arteries Build Hierarchical Branching Patterns Differently: Bottom-Up versus Top-Down. BioEssays *41*, e1800198. https://doi.org/10.1002/bies.201800198.

55. Luxán, G. (2025). Enhancing our understanding of endothelial cells. eLife *14*, e106133. https://doi.org/10.7554/eLife.106133.

56. Clevers, H. (2016). Modeling Development and Disease with Organoids. Cell *165*, 1586–1597. https://doi.org/10.1016/j.cell.2016.05.082.

57. Ma, X., Li, H., Zhu, S., Hong, Z., Kong, W., Yuan, Q., Wu, R., Pan, Z., Zhang, J., Chen, Y., et al. (2022). Angiorganoid: vitalizing the organoid with blood vessels. Vasc. Biol. *4*, R44–R57. https://doi.org/10.1530/VB-22-0001.

58. Batlle, E., and Wilkinson, D.G. (2012). Molecular Mechanisms of Cell Segregation and Boundary Formation in Development and Tumorigenesis. Cold Spring Harb. Perspect. Biol. *4*, a008227. https://doi.org/10.1101/cshperspect.a008227.

59. Madhavan, M., Nevin, Z.S., Shick, H.E., Garrison, E., Clarkson-Paredes, C., Karl, M., Clayton, B.L.L., Factor, D.C., Allan, K.C., Barbar, L., et al. (2018). Induction of myelinating oligodendrocytes in human cortical spheroids. Nat. Methods *15*, 700–706. https://doi.org/10.1038/s41592-018-0081-4.

60. Marton, R.M., Miura, Y., Sloan, S.A., Li, Q., Revah, O., Levy, R.J., Huguenard, J.R., and Pașca, S.P. (2019). Differentiation and Maturation of Oligodendrocytes in Human Three-Dimensional Neural Cultures. Nat. Neurosci. *22*, 484–491. https://doi.org/10.1038/s41593-018-0316-9.

61. Zhao, Y., Wang, X., and Wang, K. (2023). Transcription factor-mediated programming of stem cell fate. Trends Cell Biol. *33*, 621–624. https://doi.org/10.1016/j.tcb.2023.05.004.

62. Ng, A.H.M., Khoshakhlagh, P., Rojo Arias, J.E.R., Pasquini, G., Wang, K., Swiersy, A., Shipman, S.L., Appleton, E., Kiaee, K., Kohman, R.E., et al. (2021). A comprehensive library of human transcription factors for cell fate engineering. Nat. Biotechnol. *39*, 510–519. https://doi.org/10.1038/s41587-020-0742-6.

63. Skylar-Scott, M.A., Huang, J.Y., Lu, A., Ng, A.H.M., Duenki, T., Liu, S., Nam, L.L., Damaraju, S., Church, G.M., and Lewis, J.A. (2022). Orthogonally induced differentiation of stem cells for the programmatic patterning of vascularized organoids and bioprinted tissues. Nat. Biomed. Eng. *6*, 449–462. https://doi.org/10.1038/s41551-022-00856-8.

64. Chien, K.R., Zangi, L., and Lui, K.O. (2015). Synthetic Chemically Modified mRNA (modRNA): Toward a New Technology Platform for Cardiovascular Biology and Medicine. CSH Perspect. Med. *5*, a014035. https://doi.org/10.1101/cshperspect.a014035.

65. Beck, J.D., Reidenbach, D., Salomon, N., Sahin, U., Türeci, Ö., Vormehr, M., and Kranz, L.M. (2021). mRNA therapeutics in cancer immunotherapy. Mol. Cancer *20*, 69. https://doi.org/10.1186/s12943-021-01348-0.

66. Sahin, U., Karikó, K., and Türeci, Ö. (2014). mRNA-based therapeutics — developing a new class of drugs. Nat. Rev. Drug Discov. *13*, 759–780. https://doi.org/10.1038/nrd4278.

67. Han, X., Wang, M., Duan, S., Franco, P.J., Kenty, J.H.-R., Hedrick, P., Xia, Y., Allen, A., Ferreira, L.M.R., Strominger, J.L., et al. (2019). Generation of hypoimmunogenic human pluripotent stem cells. Proc. Natl. Acad. Sci. USA *116*, 10441–10446. https://doi.org/10.1073/pnas.1902566116.

68. Deuse, T., Hu, X., Gravina, A., Wang, D., Tediashvili, G., De, C., Thayer, W. O., Wahl, A., Garcia, J.V., Reichenspurner, H., et al. (2019). Hypoimmunogenic derivatives of induced pluripotent stem cells evade immune rejection in fully immunocompetent allogeneic recipients. Nat. Biotechnol. *37*, 252–258. https://doi.org/10.1038/s41587-019-0016-3.

69. Bassil, R., Shields, K., Granger, K., Zein, I., Ng, S., and Chih, B. (2021). Improved modeling of human AD with an automated culturing platform for iPSC neurons, astrocytes and microglia. Nat. Commun. *12*, 5220. https://doi.org/10.1038/s41467-021-25344-6.

70. Lach, R.S., Qiu, C., Kajbaf, E.Z., Baxter, N., Han, D., Wang, A., Lock, H., Chirikian, O., Pruitt, B., and Wilson, M.Z. (2022). Nucleation of the destruction complex on the centrosome accelerates degradation of β-catenin and regulates Wnt signal transmission. Proc. Natl. Acad. Sci. USA *119*, e2204688119. https://doi.org/10.1073/pnas.2204688119.

71. No, D., Yao, T.P., and Evans, R.M. (1996). Ecdysone-inducible gene expression in mammalian cells and transgenic mice. Proc. Natl. Acad. Sci. USA *93*, 3346–3351. https://doi.org/10.1073/pnas.93.8.3346.

72. Hahn, C., and Schwartz, M.A. (2009). Mechanotransduction in vascular physiology and atherogenesis. Nat. Rev. Mol. Cell Biol. *10*, 53–62. https://doi.org/10.1038/nrm2596.

73. Quintard, C., Tubbs, E., Jonsson, G., Jiao, J., Wang, J., Werschler, N., Laporte, C., Pitaval, A., Bah, T.-S., Pomeranz, G., et al. (2024). A microfluidic platform integrating functional vascularized organoids-on-chip. Nat. Commun. *15*, 1452. https://doi.org/10.1038/s41467-024-45710-4.

74. Kroll, K.T., Homan, K.A., Uzel, S.G.M., Mata, M.M., Wolf, K.J., Rubins, J. E., and Lewis, J.A. (2024). A perfusable, vascularized kidney organoid-on-chip model. Biofabrication *16*, 045003. https://doi.org/10.1088/1758-5090/ad5ac0.

75. Li, D., Kong, W., Hong, Y., Zhang, W., Sun, B., Wang, X., and Wang, K. (2025). Protocol for isolation and transplantation of rat pancreatic islets in the kidney capsule to treat diabetes. Star Protoc. *6*, 103486. https://doi.org/10.1016/j.xpro.2024.103486.

76. Wang, K., Wang, X., Han, C.S., Chen, L.Y., and Luo, Y. (2017). Scaffold-supported Transplantation of Islets in the Epididymal Fat Pad of Diabetic Mice. J. Vis. Exp. *125*, 54995. https://doi.org/10.3791/54995.

77. Schlaeger, T.M., Daheron, L., Brickler, T.R., Entwisle, S., Chan, K., Cianci, A., DeVine, A., Ettenger, A., Fitzgerald, K., Godfrey, M., et al. (2015). A comparison of non-integrating reprogramming methods. Nat. Biotechnol. *33*, 58–63. https://doi.org/10.1038/nbt.3070.

78. Melero-Martin, J.M., Khan, Z.A., Picard, A., Wu, X., Paruchuri, S., and Bischoff, J. (2007). In vivo vasculogenic potential of human blood-derived endothelial progenitor cells. Blood *109*, 4761–4768. https://doi.org/10.1182/blood-2006-12-062471.

79. Zheng, G.X.Y., Terry, J.M., Belgrader, P., Ryvkin, P., Bent, Z.W., Wilson, R., Ziraldo, S.B., Wheeler, T.D., McDermott, G.P., Zhu, J., et al. (2017). Massively parallel digital transcriptional profiling of single cells. Nat. Commun. *8*, 14049. https://doi.org/10.1038/ncomms14049.

80. McGinnis, C.S., Murrow, L.M., and Gartner, Z.J. (2019). DoubletFinder: Doublet Detection in Single-Cell RNA Sequencing Data Using Artificial Nearest Neighbors. Cell Syst. *8*, 329–337.e4. https://doi.org/10.1016/j.cels.2019.03.003.

81. Hao, Y., Hao, S., Andersen-Nissen, E., Mauck, W.M., Zheng, S., Butler, A., Lee, M.J., Wilk, A.J., Darby, C., Zager, M., et al. (2021). Integrated analysis of multimodal single-cell data. Cell *184*, 3573–3587.e29. https://doi.org/10.1016/j.cell.2021.04.048.

Please cite this article in press as: Gong et al., Rapid generation of functional vascular organoids via simultaneous transcription factor activation of endothelial and mural lineages, Cell Stem Cell (2025), https://doi.org/10.1016/j.stem.2025.05.014

CellPress

STAR★METHODS

KEY RESOURCES TABLE

REAGENT or RESOURCE	SOURCE	IDENTIFIER
Antibodies		
APC-anti-CD31	Biolegend	RRID: AB_1877151; Cat# 303116
APC-anti-CD140b	Biolegend	RRID: AB_2162787; Cat# 323608
FITC anti-human CD73	Biolegend	RRID: AB_2561808; Cat# 344015
PE anti-human CD144 (VE-CAD)	ThermoFisher	RRID: AB_763438; Cat# 12-1449-82
PE anti-human CD184 (CXCR4)	Biolegend	RRID: AB_314611; Cat# 306505
PE anti-human CD62E (ESelectin)	ThermoFisher	RRID: AB_11217891; Cat# 12-0627-41
PE anti-CD54 (ICAM-1)	ThermoFisher	RRID: AB_10597124; Cat# 12-0549-41
PE anti-CD106 (VCAM-1)	BioLegend	RRID: AB_314561; Cat# 305805
Rabbit anti-human ETV2	Abcam	RRID: AB_3665369; Cat# Ab181847
Mouse anti-NKX3.1	Santa Cruz	RRID: AB_3665370; Cat# Sc-393190
Goat anti-Brachyury (T)	R&D	RRID: AB_2200235; Cat# AF2085
Goat anti-human PDGFR beta	R&D	RRID: AB_355339; Cat# AF385
Mouse anti-human CD31	Santa Cruz	RRID: AB_629040; Cat# sc-53411
Rabbit anti-human CD31	Abcam	RRID: AB_1523298; Cat# Ab76533
Rat anti-mouse CD31	BD Pharmingen	RRID: AB_393571; Cat# 550274
Rabbit anti-human Alpha Smooth Muscle Actin (a-SMA)	Abcam	RRID: AB_2223021; Cat# Ab5694
Rabbit anti-smooth muscle myosin heavy chain 11	Abcam	RRID: AB_2890982; Cat# Ab133567
Human Podocalyxin Antibody	R&D	RRID: AB_354920; Cat# AF1658
Mouse anti-human vimentin	Abcam	RRID: AB_306239; Cat# Ab8069
Rabbit anti-Collagen IV	Abcam	RRID: AB_305584; Cat# Ab6586
Mouse anti-human SOX17	ThermoFisher	RRID: AB_2725396; Cat# MA5-24885
Rabbit anti-NR2F2	Abcam	RRID: AB_2895604; Cat# Ab211777
Biotinylated Ulex Europaeus Agglutinin I (UEA-I)	Vector Laboratories	RRID: AB_2336766; Cat# B-1065-2
Rhodamine labeled Ulex Europaeus Agglutinin I (UEA-I)	Vector Laboratories	RRID: AB_2336767; Cat# FL-1061
Anti-Insulin antibody	Abcam	RRID: AB_306130; Cat# Ab7842
Donkey anti-mouse IgG, AlexaFluor 647	ThermoFisher	RRID: AB_162542; Cat# A-31571
Donkey anti-mouse IgG, AlexaFluor 568	ThermoFisher	RRID: AB_11180865; Cat# A-10037
Donkey anti-mouse IgG, AlexaFluor 488	ThermoFisher	RRID: AB_141607; Cat# A-21202
Donkey anti-rabbit IgG, AlexaFluor 568	ThermoFisher	RRID: AB_2534017; Cat# A-10042
Goat anti-rabbit IgG, AlexaFluor 488	ThermoFisher	RRID: AB_2576217; Cat# A-11034
Donkey anti-goat IgG, AlexaFluor 568	ThermoFisher	RRID: AB_2534104; Cat# A-11057
Donkey anti-goat IgG, AlexaFluor 488	Invitrogen	RRID: AB_2556666; Cat# SA5-10086
Biological samples		
BJ273-iPSCs (BJ-iPSCs)	Schlaeger et al.[77]	N/A
Endothelial colony-forming cells (ECFCs)	Melero-Martin et al.[78]	N/A
Chemicals, peptides, and recombinant proteins		
PiggyBac super transposase	SBI	Cat# PB210PA-1
Y27632	Selleckchem	Cat# S1049
CHIR99021	Sigma-Aldrich	Cat# SML1046-25MG
Puromycin	InvivoGen	Cat# ant-pr-1

(*Continued on next page*)

Please cite this article in press as: Gong et al., Rapid generation of functional vascular organoids via simultaneous transcription factor activation of endothelial and mural lineages, Cell Stem Cell (2025), https://doi.org/10.1016/j.stem.2025.05.014

Continued

REAGENT or RESOURCE	SOURCE	IDENTIFIER
100X glutamax	Thermofisher	Cat# 35050061
Doxycycline hyclate	Sigma-Aldrich	Cat# D9891-10G
Gelatin from porcine skin	Sigma-Aldrich	Cat# G2500-500G
L-Ascorbic acid phosphate	Millipore Sigma	Cat# A8960-5G
Penicillin-Streptomycin (P/S)	Thermofisher	Cat# 15140122
EGF Human	ProSpec	Cat# CYT-798
FGF 2 Human (147 a.a.)	ProSpec	Cat# CYT-557
VEGF Human	ProSpec	Cat# CYT-241
Human TNF Alpha	PeproTech	Cat# 300-01A
Recombinant Human BMP-4 (*E. coli* derived)	PeproTech	Cat# 120-05ET-10UG
Forskolin	Millipore-Sigma	Cat# F3917-10MG
Streptavidin, Texas Red	Vector Laboratories	Cat# SA-5006-1
Matrigel	Corning	Cat# 354277
Collagen	Trevigen	Cat# 3442-050-01
Fibrinogen	Sigma-Aldrich	Cat# F8630-1G
Human fibronectin	Millipore-Sigma	Cat# F0895-2MG)
Critical commercial assays		
Neon Electroporation Kit	Invitrogen	Cat# MPK1009
Chromium Next GEM Single Cell Reagent Kits	10xgenomics	PN-1000128 and PN-1000127
Library prep kit	10xgenomics	PN-1000213
SYBR™ Green Cells-to-CT™ Kit	Thermofisher Scientific	Cat# 4402954
RNeasy kit	Qiagen	Cat# 74106
Deposited data		
RNA sequencing data from 2D-iECs, 2D-iMCs, VO-iECs, and VO-iMCs	This paper	GEO: GSE281002
scRNA sequencing data	This paper	GEO: GSE281002
Experimental models: Organisms/strains		
Athymic nude mice (Foxnl/nu mice)	Envigo	N/A
NOD.Cg-Prkdcscid Il2rgtm1Wjl/SzJ (# 005557)	Jackson	RRID: IMSR_JAX:005557
Oligonucleotides		
Primers for qPCR, see Table S1	This paper	N/A
Recombinant DNA		
Dox-inducible ETV2 PiggyBac	Luo et al.[40]	N/A
Dox-inducible NKX3.1 PiggyBac	Lee et al.[31]	N/A
Software and algorithms		
Trimmomatic v.0.39		N/A
Illumina's bcl2fastq 2.17 software		N/A
STAR aligner v.2.7.11b		N/A
DESeq2 R package		N/A
GeneSCF		N/A
Cellranger count	Zheng et al.[79]	N/A
DoubletFinder package (version 2.0.4)	McGinnis et al.[80]	N/A
Seurat package (version 5.1.0)	Hao et al.[81]	N/A

Please cite this article in press as: Gong et al., Rapid generation of functional vascular organoids via simultaneous transcription factor activation of endothelial and mural lineages, Cell Stem Cell (2025), https://doi.org/10.1016/j.stem.2025.05.014

CellPress

EXPERIMENTAL MODEL AND STUDY PARTICIPANT DETAILS

Animals

Immunodeficient male nude mice (Foxn1/nu) aged 6 weeks were purchased from Envigo RMS LCC, and immunodeficient male NOD-SCID mice (NOD.Cg-*Prkdc*^{scid}*Il2rg*^{tm1Wjl}/SzJ) aged 6 weeks were purchased from The Jackson Laboratory. Mice were housed at 22 ± 2 °C, 40-60 humidity, under the standard laboratory conditions with free access to rodent feed and water, in the barrier mouse facility. All experiments were conducted at Boston Children's Hospital in compliance with protocols approved by the Institutional Animal Care and Use Committee (IACUC).

Cell lines

The BJ273 iPSC line was sourced from Boston Children's Hospital's Stem Cell Core. Dox-ETV2 and Dox-NKX3.1-iPSCs were engineered from this parental BJ273 line. All iPSCs were cultured in mTeSR Plus medium (STEMCELL Technologies) with 5 μM Y27632 rock inhibitor (Selleck-chem) on Matrigel-coated (Corning) 6-well plates (Gene Clone). Human endothelial colony-forming cells (ECFCs), human umbilical vein endothelial cells (HUVECs), and human saphenous vein smooth muscle cells (vSMCs; kindly donated by Dr. Joyce Bischoff, Boston Children's Hospital) served as primary cell controls. ECFCs and HUVECs were cultured in ECGM2 (Lonza) supplemented with 20% FBS (Genesee) without hydrocortisone. vSMCs were cultured in SmGM-2 medium (Lonza) on 1% gelatin-coated plate (Sigma-Aldrich).

METHOD DETAILS

Generation of doxycycline-inducible ETV2 and NKX3.1 iPSC lines

Doxycycline-inducible ETV2 (dox-ETV2) and NKX3.1 (dox-NKX3.1) iPSC lines were generated using the piggyBac (PB) transposon and transposase system as previously described.[31,40] In brief, 1 μg of Super transposase (SBI System Biosciences, PB210PA-1) and 5 μg of PB dox-ETV2 or NKX3.1 transposon were transfected into 2 million BJ273 iPSCs via the Neon electroporation system (Invitrogen, MPK10096) with parameters set to 1150 V for pulse voltage, 30 ms pulse width, and two pulses. Each reaction included 3 mL of electrolytic buffer and 100 μL of resuspension buffer R in 100 μL reaction tips. Post-electroporation, cells were seeded on Matrigel-coated dishes in mTeSR Plus medium (STEMCELL Technologies, 100-0276) with 5 μM Y27632 (Selleckchem, S1049), and puromycin selection at 0.5 μg/mL (InvivoGen, ant-pr-1) was applied. Positive iPSC clones were manually collected, and their pluripotency and doxycycline responsiveness were confirmed by qPCR and immunostaining assays.

Generation of vascular organoids

Doxycycline-inducible Protocol

Dox-ETV2 and dox-NKX3.1 h-iPSCs were initially dissociated into single cells using TrypLE Select (Thermo Fisher Scientific, 12563-029) and plated onto Matrigel-coated 6-well plates in mTeSR plus medium with 5 μM Y27632. After 24 hours, when cells reached 30-40% confluency, the medium was replaced with S1 medium, containing basal medium supplemented with 6 μM CHIR99021 (Sigma-Aldrich, SML1046). The basal medium included Advanced DMEM/F-12 (Thermo Fisher Scientific, 12634010), 1x GlutaMax (Thermo Fisher Scientific, 35050061), 60 μg/mL L-ascorbic acid phosphate (Thermo Fisher Scientific, A8960-5G), and 0.4x P/S. After 24 hours, the medium was replaced again, and culture continued for another 24 hours to yield mesodermal progenitor cells (MePCs).

MePCs were then dissociated, and 2 million MePCs from dox-ETV2 and 2 million from dox-NKX3.1 h-iPSCs were combined and cultured in 6-well suspension plates in S2 medium. This medium consisted of basal medium supplemented with 0.5 μg/mL Doxycycline Hyclate (Sigma, D9891), 10 ng/mL EGF (ProSpec, CYT-798), 50 ng/mL FGF-2 (ProSpec, CYT-557), and 50 ng/mL VEGF (ProSpec, CYT-241). Plates were placed on an orbital shaker at 100 rpm, with daily medium changes. After 3 days, the VOs were obtained.

modRNA protocol

BJ273 hiPSCs were first differentiated into MePCs, as in the doxycycline-inducible protocol. MePCs were then dissociated into single cells and transfected with modRNA: 2 million MePCs were transfected with 1 μg modETV2, and another 2 million with 1 μg modNKX3.1. Chemically modified RNAs encoding ETV2 and NKX3.1 were generated by TriLink Bio Technologies LLC through in vitro transcription, following a method previously described.[30,31] Briefly, T7 RNA polymerase-mediated transcription was conducted from a linearized DNA template with 5′ and 3′ UTRs and a poly-A tail; capped mRNAs were created using CleanCap Cap1 AG trimer, and additional processing steps included deoxyribonuclease treatment, phosphatase treatment to reduce immune response, and final purification on a silica membrane.

Following transfection, cells were cultured in a 6-well suspension plate in S2 medium, consisting of basal medium supplemented with 10 ng/mL EGF (ProSpec, CYT-798), 50 ng/mL FGF-2 (ProSpec, CYT-557), and 50 ng/mL VEGF (ProSpec, CYT-241). Plates were placed on an orbital shaker (100 rpm), with daily medium changes. After 3 days, modRNA vascular organoids (modRNA-VOs) were obtained.

VO embedding in collagen/Matrigel matrix

To embed VOs, one well of a 6-well plate was used to seed two 12-well plates, with each 12-well plate holding 40–60 VOs per well. Each plate required 12 mL of collagen I–Matrigel solution, with 6 mL per layer (0.5 mL per well). Matrigel was thawed on ice, mixed

Please cite this article in press as: Gong et al., Rapid generation of functional vascular organoids via simultaneous transcription factor activation of endothelial and mural lineages, Cell Stem Cell (2025), https://doi.org/10.1016/j.stem.2025.05.014

with collagen I, and 0.5 mL of the mixture was added to each well, followed by incubation at 37 °C for 2 hours to solidify. Optimal VO density was maintained to promote vascular network formation while avoiding fusion.

For embedding preparation, VOs were pipetted into 15-mL tubes, collected by gravity, and washed twice with StemPro-34 SFM (Gibco, 10639011). For the second layer, PureCol collagen I (Advanced BioMatrix, 5005) was combined with Matrigel on ice, and VOs were resuspended in this solution. The first layer in the 12-well plates was then overlaid with 0.5 mL of the VO-collagen I-Matrigel solution per well. Plates were gently rocked to evenly distribute VOs, and incubated at 37 °C for 2 hours for gel solidification.

After solidification, prewarmed (37 °C) StemPro-34 SFM complete medium with 15% FBS, 100 ng/mL VEGF-A, and 100 ng/mL FGF-2 was added to each well to support blood vessel differentiation. Medium was refreshed every other day, and the blood vessel networks were analyzed using staining protocols on day 5.

Isolation of iECs and iMCs from VOs

At designated time points post-differentiation, VOs were dissociated into single cells and sorted into CD31+ and CD31− populations using anti-human CD31 antibody-coated magnetic beads (DynaBeads, Thermo Fisher Scientific, 11155D). CD31+ iECs were cultured on 10-cm gelatin-coated dishes (1% gelatin) in EGM-2 medium, prepared by supplementing Endothelial Cell Growth medium 2 kit into basal medium (excluding hydrocortisone; PromoCell, C22111) with 1x P/S. CD31− iMCs were expanded on 10-cm dishes in SmGM-2 medium (Lonza, CC-3182).

Quantitative reverse transcription PCR

Total RNA was isolated using either the RNease kit (Qiagen, 74106) or SYBR™ Green Cells-to-CT™ Kit (Thermo Fisher, 4402954). cDNA synthesis followed using either reverse transcriptase III (Thermo Fisher, 4368814) or the SYBR™ Green Cells-to-CT™ Kit. Quantitative PCR was performed with SYBR Green Master Mix (Thermo Fisher, A25776) on the QuantStudio™ 3 Real-Time PCR System (Thermo Fisher, A28567). Gene expression levels were normalized to GAPDH as a reference, with primer sequences listed in Table S1.

Flow cytometry

Cells were dissociated with TrypLE, washed in phosphate-buffered saline (PBS) with FACS buffer (1x PBS, 0.5% BSA, 0.2 mM EDTA), and stained with fluorochrome-conjugated antibodies for 20 minutes at 4°C. After three washes, cells were resuspended in FACS buffer and analyzed on a BD Accuri™ C6 Plus flow cytometer (BD Biosciences), with data processed in FlowJo 10.10 (BD Biosciences). Detailed antibody information is provided in key resources table.

Immunofluorescence staining

Immunofluorescence staining of cells

Cells were seeded at $2x10^4$ cells/cm^2 on tissue culture-treated eight-well chamber slides (ibidi USA, Fisher Scientific, 50-305-795 or NC1535706). Cells were fixed with 4% paraformaldehyde (PFA), permeabilized with either 100% cold methanol at -20°C or 0.2% Triton X-100 in PBS for 15 minutes, and blocked with 10% BSA for 30 minutes at room temperature. Primary antibodies were applied for 1 hour at room temperature or overnight at 4°C, followed by three PBS washes. Secondary antibodies and DAPI were added for 30 minutes at room temperature, and cells were mounted with DAKO fluorescence mounting medium (Agilent, S302380-2). Antibody details are provided in key resources table.

Whole-mount staining of VOs

VOs were fixed in 4% PFA for 1 hour, rinsed in PBS, and blocked with 5% BSA in PBS for 1 hour. Primary antibodies in blocking buffer (5% BSA in PBS) were applied overnight at 4°C on a rocking shaker. After three 10-minute PBS washes, organoids were incubated with secondary antibodies and DAPI for 2 hours at room temperature, followed by PBS washes.

Whole-mount CUBIC clearing and staining of VOs

Mature VOs, which remained embedded in ECM until fixation, were carefully dissected under sterile conditions using sterile 30-gauge needles to minimize residual matrix. Dissected VOs were then fixed in 4% PFA for 24 hours, rinsed in PBS, and treated with a 1:1 dH2O R1 solution (35% dH2O, 15% Triton X-100, 25% quadrol, 25% urea) with three liquid exchanges over 6 hours, then incubated in R1 for 24 hours. VOs were washed three times in IHC buffer (PBS with 0.1% Triton X-100, 0.1% BSA, 0.01% sodium azide) for 2 hours each, then incubated in primary antibodies for 48 hours at room temperature in IHC buffer. After three washes, VOs were incubated in IHC buffer with secondary antibodies overnight, washed in PBS, and cleared in CUBIC R2 (15% dH2O, 0.1% Triton X-100, 25% urea, 50% sucrose). Cleared VOs were transferred to an incubation chamber, mounted on slides, and imaged on a Zeiss 880 confocal with Fast Airyscan.

Sprouting assay

VOs, generated with a GFP reporter in the ETV2 line to label iECs, were collected on day 5 and embedded in fibrin gel (5 mg/mL fibrinogen, Sigma-Aldrich, F8630; 0.5 U/mL thrombin, Sigma, T-9549). A 100-μL fibrin gel/VO construct was placed in the center of a 35-mm glass-bottom dish (MatTek, P35G-1.5-10-C) and incubated at 37°C for 10 minutes to solidify. Constructs were cultured for 1 day, with 10 μM DAPT added in indicated experiments during embedding. GFP+ sprouts were imaged with an inverted fluorescence microscope, and sprout lengths were measured using ImageJ.

Please cite this article in press as: Gong et al., Rapid generation of functional vascular organoids via simultaneous transcription factor activation of endothelial and mural lineages, Cell Stem Cell (2025), https://doi.org/10.1016/j.stem.2025.05.014

Tube formation assay

ECs (ECFCs, 2D-iECs, or VO-iECs) were seeded in a 96-well plate on top of 50 μL of solidified Matrigel in EGM-2 medium. After 6 hours, cells were incubated with 1 μM Calcein-AM (BioLegend, 425201) for 10 minutes and imaged using a fluorescence microscope. Branch numbers were quantified with ImageJ.

Leukocyte adhesion molecule assay

Cells were seeded on gelatin-coated 48-well plates (10^5 cells per well) in EGM-2 medium. At confluency, cells were treated with or without 10 ng/mL TNF-α (PeproTech, 300-01A) for 5 hours, then lifted and stained with anti-ICAM-1, anti-E-selectin, or anti-VCAM-1 antibodies for flow cytometry analysis.

Animal experiments

All animal procedures were approved by the Institutional Animal Care and Use Committee at Boston Children's Hospital in an AAALAC-accredited facility.

VO transplantation in the kidney capsule

In NOD-SCID mice, 1,000 tdTomato/luciferase-labeled VOs, with luciferase expression driven by the ETV2 line to track iECs, were transplanted under the left kidney capsule through a small incision. Bioluminescence was monitored weekly for 4 weeks using the IVIS system following administration of luciferin (150 mg/kg). Some grafts were explanted at 2 weeks for histological analysis with H&E and immunofluorescent staining.

To assess vascular perfusion, mice received a tail vein injection of biotinylated Ulex Europaeus Agglutinin I (UEA-I; 50 μg in PBS; Vector Laboratories, B-1065-2) 30 minutes prior to euthanasia. UEA-I selectively binds to human ECs, allowing the identification of perfused human vessels in vivo. Following tissue harvest and fixation, Streptavidin Texas Red (Vector Laboratories, SA-5006-1) was applied to the histological sections of the grafts to visualize UEA-1+ vessels. Sections were also stained with human-specific anti-CD31 to confirm the presence of human ECs.

Mouse hind limb ischemia model

Diabetes was induced in athymic nude mice via a single intraperitoneal injection of streptozotocin (220 mg/kg), with blood glucose levels checked to confirm hyperglycemia. Four days later, ischemia was induced by ligating the femoral artery and vein. Immediately after ligation, mice received either 1,000 VOs, with luciferase expression driven by the ETV2 line to track iECs, or 2 × 10^6 cells (luciferase-iECs + iMCs in a 1:1 ratio) suspended in 50 μL ice-cold Matrigel (Corning, 356237) injected into the ischemic muscle. Bioluminescence was monitored at indicated time points using the IVIS system following administration of luciferin (150 mg/kg). Blood flow recovery in the hind limbs was assessed using laser Doppler imaging pre-surgery and on postoperative days 0, 1, 3, 5, 7, 10, and 14, with relative blood flow calculated as the ratio of the operated to contralateral limb.

Murine pancreatic islets transplantation model

Pancreatic islets were isolated from C57BL/6 mice, digested with collagenase, and purified as previously described.[75,76] Isolated islets were combined with 1,500 VOs, washed in PBS, and resuspended in 50 μL PBS for transplantation. Non-fasting blood glucose was monitored weekly for up to 4 months to evaluate graft function. Two days before the end time point, mice underwent nephrectomy of the kidney containing the graft to confirm that normoglycemia was graft-dependent.

Bulk RNA sequencing

Bulk RNA sequencing was performed h-iECs and h-iMCs generated via both 2D and VO protocols, with three biological replicates per group. Total RNA extraction, library preparation, and sequencing were conducted by GENEWIZ (Azenta Life Sciences) using the Qiasymphony RNA kit (Qiagen, 931636) for RNA extraction. Libraries were prepared with mRNA enrichment, fragmentation, cDNA synthesis, end repair, adaptor ligation, and PCR enrichment, then sequenced on the Illumina HiSeq 2500 platform (2 ×150 paired-end). Sequencing data were processed with Illumina's bcl2fastq software for fastq conversion and de-multiplexing.

Raw reads were quality-checked and trimmed with Illumina v.0.39 to remove low-quality bases and adapter sequences, then aligned to the *Homo sapiens* reference genome (ENSEMBL) using STAR aligner v.2.7.11b. Unique gene hit counts were calculated with featureCounts (Subread package v.2.0.7) from exon regions, and differential expression analysis was conducted with DESeq2, using the Wald test to generate p-values and Log_2 fold changes. Genes with adjusted p-values < 0.05 and absolute Log_2 fold changes > 1 were considered differentially expressed. Gene ontology (GO) analysis of significant genes was performed with GeneSCF software, and principal component analysis (PCA) on the top 500 genes was visualized with the "plotPCA" function in DESeq2 using Euclidean distance as the distance metric.

Single-cell RNA sequencing

Cell and library preparation

Cells were dissociated with TrypLE (3 minutes at 37°C for cells, 10 minutes for VOs), filtered through a FACS cell strainer, and prepared for single-cell RNA sequencing using the Chromium Next 10X Genomics platform (10xGenomics, PN-1000128, PN-1000127) per the manufacturer's protocol. DNA quantification and quality control were performed using a Qubit 2.0 Fluorometer and Agilent TapeStation D5000 at Harvard's core facility. RNA sequencing libraries were prepared with the dual index kit (10xGenomics, PN-1000213) and validated using the Agilent TapeStation D1000.

Please cite this article in press as: Gong et al., Rapid generation of functional vascular organoids via simultaneous transcription factor activation of endothelial and mural lineages, Cell Stem Cell (2025), https://doi.org/10.1016/j.stem.2025.05.014

Illumine sequencing

Sequencing was conducted by Medgenome on an Illumina Novaseq 6000, generating 150 paired-end reads (approximately 503 GB). The CellRanger software (10x Genomics) processed raw BCL files to produce FASTQ files and count matrices, utilizing the "cellranger count" module for feature-barcode matrices.

Dataset quality control

Data were processed using 10x Genomics Cell Ranger (v8.0.1) and aligned to the GRCh38 human genome (refdata-gex-GRCh38-2020-A). Quality control was performed in Seurat (v5.1.0), removing potential doublets identified by DoubletFinder (v2.0.4) and filtering for cells with 200–9,000 unique genes and <20% mitochondrial content to ensure high dataset integrity.

Cell clustering

Seurat (v5.1.0) was used for data normalization, scaling, and clustering. Feature expression was normalized with "LogNormalize" and scaled with "ScaleData." The top 2,000 variable genes were identified with "FindVariableFeatures" for PCA. A K-nearest neighbor (KNN) graph, based on the first 15 principal components, was constructed with "FindNeighbors," and cells were clustered with "FindClusters." Differentially expressed genes (DEGs) were identified using "FindAllMarkers."

Microscopy

Fluorescent images were captured on a Zeiss Axio Observer Z1 inverted microscope with an AxioCam MRc5 using a 20X objective, while 5X or 10X objectives were used for phase contrast imaging. Whole-mount VO staining was analyzed on a Zeiss LSM880 Laser Scanning Confocal microscope. Image analysis was performed using ZEN 3.6 (blue edition), ZEN 2.3 SP1, and ImageJ2 (2.9.0/1.53t).

QUANTIFICATION AND STATISTICAL ANALYSIS

All experiments were independently repeated at least three times with consistent results. Micrographs in the figures represent experiments conducted on three or more occasions. Data are reported as means ± standard error of the mean (s.e.m.) unless specified otherwise. Statistical analyses included unpaired two-tailed Student's t-tests for two-group comparisons and one-way ANOVA with Bonferroni correction for multiple group comparisons. No exclusion criteria were applied. All calculations were performed using GraphPad Prism v.10, with significance set at $P < 0.05$.